Petrography descriptions and U-Pb zircon datasets from the Archean Pavas Block, Precambrian of Uruguay

Henri Masquelin, Tahar Aïfa, Fernando Scaglia, Miguel a S Basei, Miguel A.S. Basei

Data in Brief 37 (2021) 107179

Contents lists available at ScienceDirect

Data in Brief

journal homepage: www.elsevier.com/locate/dib

Data Article

Petrography descriptions and U-Pb zircon datasets from the Archean Pavas Block, Precambrian of Uruguay

Henri Masquelin[a,*], Tahar Aïfa[b], Fernando Scaglia[c], Miguel A.S. Basei[d]

[a] Instituto de Ciencias Geológicas, Facultad de Ciencias – UdelaR, Iguá 4225 p12 ala sur, 11400 Montevideo, Uruguay
[b] Univ. Rennes, CNRS, Géosciences Rennes – UMR6118, Campus Beaulieu, 35042 Rennes, France
[c] Post-graduate Course, PEDECIBA Geosciences, Uruguay
[d] Centro de Pesquisas Geocronológicas, Universidade de São Paulo, Brazil

ARTICLE INFO

Article history:
Received 7 May 2021
Accepted 26 May 2021
Available online 29 May 2021

Keywords:
Gneiss complex
Nico Pérez Terrane
Zircon texture
Orosirian
U-Pb geochronology

ABSTRACT

This database is a geological and geochronological compilation made to study a small Archean/Paleoproterozoic block located in the centre of the Precambrian rock exposition of Uruguay. Petrographic and field outcrops data supporting the samples from which the zircons for textural analysis and U-Pb dating (LA-ICP-MS) come are presented at first with their descriptions. The first table (1) contains the new U-Pb isotopic data. The second table (2) presents a correlation of textures from different zircon samples. The last table (3) contains an inventory of different U-Pb ages found in antecedents. All these data are associated with the paper entitled: "The Archean Pavas Block in Uruguay: extension and tectonic evolution based on LA-ICP-MS U-Pb ages and airborne geophysics".

DOI of original article: 10.1016/j.jsames.2021.103364
* Corresponding author.
E-mail address: emasquelin@fcien.edu.uy (H. Masquelin).
Social media: (H. Masquelin)

https://doi.org/10.1016/j.dib.2021.107179

Specifications Table

Subject	Earth and Planetary Sciences, Geology.
Specific subject area	Geochronology, U-Pb dating system.
Type of data	Figures with descriptive text and tables.
How data were acquired	Petrographic microscope, binocular microscope, SEM cathodoluminescence, IsoplotR software (Vermeesch 2018), QGis (GNU) software, Oasis-Montaj 8.3.0© (Geosoft Inc.). Laser ablation ICP-MS mass spectrometry using the Excimer laser of ArF gas (193 nm) coupled to the Neptune^{TM} High-Resolution Multi-collector ICP-MS at the Geochronological Laboratory of the Geosciences Institute from the University of São Paulo (Brazil).
Data format	Raw (Photos and U-Pb data), analysed, processed, and filtered.
Parameters for data collection	Representative sample collection for the La China Complex and the Campanero Gneisses for U-Pb geochronology. Petrographic thin sections were prepared. Zircons mounted in epoxy resin were described.
Description of data collection	Petrography and U-Pb zircon analyses of the granitic – gneisses and migmatites of the Pavas Block, a segment composed of pre-Neoproterozoic basement rocks westward the Neoproterozoic Dom Feliciano Belt.
Data source location	Zapicán, Route 40, Penitente, El Soldado; Lavalleja Department; Uruguay. All the cartographic coordinates in the text are in the reference system EPSG 32721 (UTM wgs84 21S). Zapicán (Lat. -33.40887, Long. -54.90875; Lat. -33.55428; Long. -54.89335) Route 40 (Lat. -33.74979, Long. -55.09939; Lat. -33.75518, -54.99020) Penitente (Lat. -34.33662, Long. -55.10061) El Soldado (Lat. -34.14855, Long. -55.26246) Primary data sources of data in antecedent are shown in the last column of Table III (see Reference list).
Data accessibility	Data are available within the article and in the repository. Repository name: Mendeley Data identification number: http://dx.doi.org/10.17632/7hk685mzjn.1 Direct URL to data: http://dx.doi.org/10.17632/7hk685mzjn.1
Related research article	H. Masquelin, T. Aïfa, F. Scaglia, M.A.S. Basei, The Archean Pavas Block in Uruguay: extension and tectonic evolution based on LA-ICP-MS U-Pb ages and airborne geophysics, J. South American Earth Sciences. In Press.

Value of the Data

- U-Pb isotopic data in zircon confirm the presence in Uruguay of Archean metamorphic crystallisation rocks without subsequent recycling.
- These data can be helpful to establish correlations between accreted terranes within the Brasiliano amalgamation.
- They can be used together with other U-Pb and Lu-Hf isotopic data to refine model ages and understand the origin of the protoliths.
- The exploitation of these U-Pb isotopic analyses varies between 94% and 38% depending on each sample since many spots have a high content of common Pb.
- Petrographic data of the La China Complex encompasses more than the samples that were dated because it attempts to show the geodiversity within this gneissic complex to construct a more detailed geological map.

1. Data Description

1.1. Petrographic data

This petrographic description primarily represents the dated samples but not exclusively. Almost these rock samples come from a migmatite complex and range from highly plastically deformed to slightly affected by strain. The most abundant rocks are orthogneisses with amphibo-

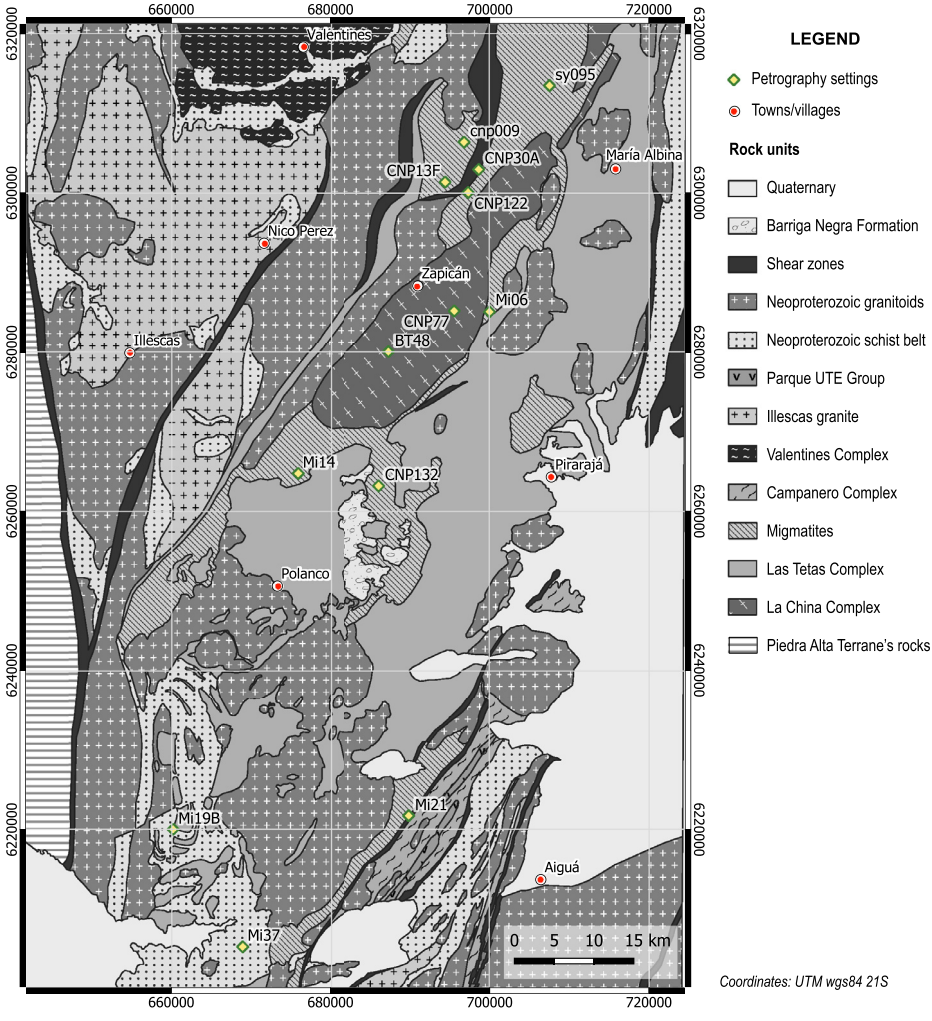

Fig. 1. Geological location of the petrographic and zircon isotopic samples in the Pavas Block (central Uruguay).

lite boudins or schlieren. These rocks usually show pegmatite injections. Hydrothermally altered granitoids include grey metatonalites that enclose some xenoliths of retrogressed mafic rocks. The gneissic layering (SL) and mineral lineation (Lm) was added to each sample when available. The gneisses generally show amphibolite facies metamorphic mineral assemblages. However, different minerals and microstructures indicate widespread hydrothermalism in the greenschist facies. Interspersed banded felsic gneisses and amphibolites are shown. The studied outcrops are showing in the map (Fig. 1).

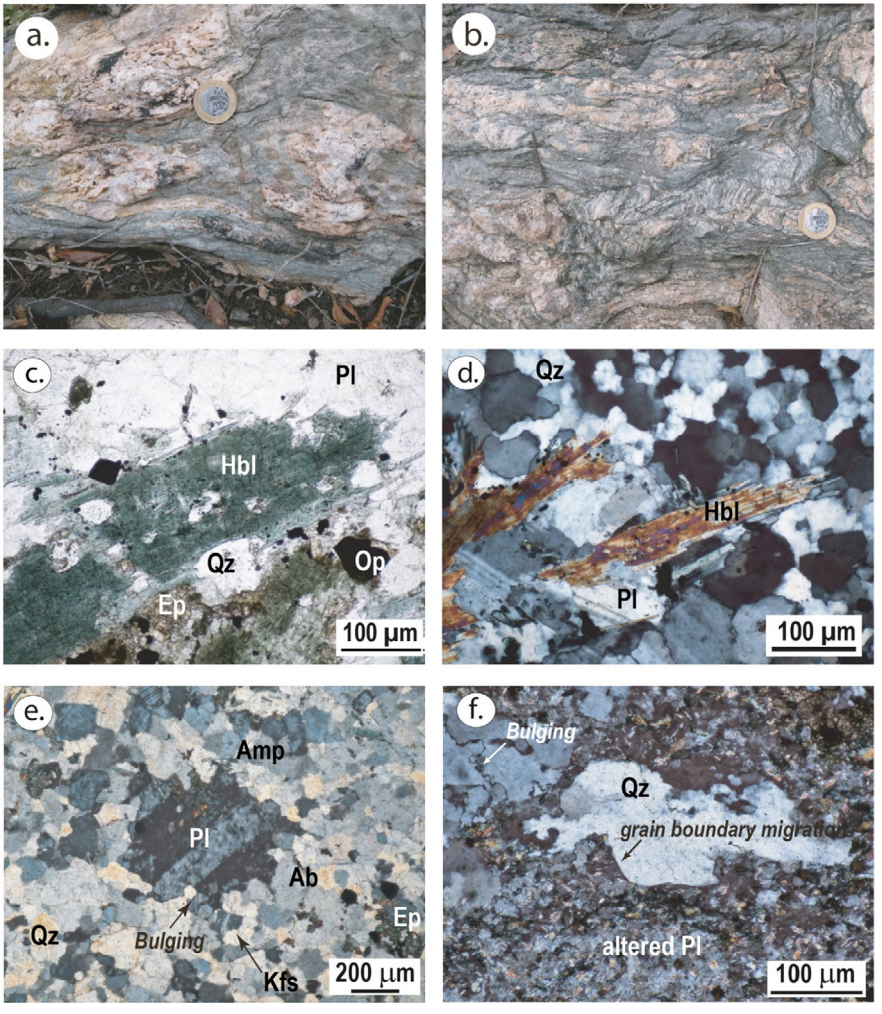

Fig. 2. a) Amphibole-bearing orthogneiss with amphibolite blocks (CNP13F) (a to d), containing b) Ep+Hbl+Pl mineral assemblage; c) Polygonal texture and grain-boundary migration recrystallisation on Qz; d) Epidote net texture; e) Mus+Ep+Pl orthogneiss (CNP77) (e to h), with f) Ep-Mus hydrothermal veins; g) Saussuritic plagioclase, and epidote veins; h) Detailed mineral inclusions within the saussurite; Mineral abbreviations follow the criteria of Whitney and Evans [5].

1.2. Petrographic description of dated samples

1.2.1. Sample CNP13F

Amphibole-bearing orthogneiss with sharp-angled boudins of amphibolite (Fig. 2a; coord.: x = 681875; y = 6251285). The rotated boudins allow deducing a dextral kinematic sense (Lm = 20/190; SL = 50/45). In the thin section, the orthogneiss texture is granoblastic lobate equigranular (~100-200 µm grain-sized) (Fig. 2b). It is composed of brown to green amphibole (tschermakite, hornblende), Ca-plagioclase, quartz, epidote (Fig. 2c). Accessories include zircon, opaques, and apatite. Epidote developed a skeletal or net texture around polygonal plagioclase grains (Fig. 2d). There are domains almost entirely composed of quartz which contain hornblende and plagioclase. The “chessboard” pattern is common on quartz sub-fabric [1].

1.2.2. Sample CNP77

Flat-lying composite layered rock (Fig. 2e; coord.: x=695628; y=6285289) which separates into (i) a coarse-grained white augen gneiss and (ii) a biotite-bearing mylonite (SL: 150/18; Lm: 5/230). The coarse-grained rock dominates in the thin section. Epidote-muscovite-bearing quartz veins crosscut the layering both discordant and concordantly (Fig. 2f). The texture is porphyroblastic heterogranular. Crystal-size is c. 500 µm on average. The coarse-grained rock (i) is composed of quartz (35%), poikiloblastic saussuritic Ca-plagioclase (50%), microcline, muscovite, and epidote in veins (Fig. 2g). A detailed overview shows minute grains of well-crystallised zoisite and muscovite (Fig. 2h). Carlsbad/albite twinned oligoclase (An24) is present. Accessory minerals are pale-brown biotite, opaque minerals, titanite, apatite and zircon. Dynamic recrystallisation of quartz is due to diffusion-assisted grain-boundary migration [1]. Patchy-perthite feldspar is present in the porphyroclasts.

1.2.3. Sample Mi21

Fine-grained amphibole-bearing orthogneiss crosscut by Kfs-rich granitic veins (coord.: x = 689924; y = 6221711) (Fig. 3a). A low-temperature mylonitization/cataclasis (Sm: 33/30) crosscut the high-temperature layering (Fig. 3b). The texture is grano-nematoblastic heterogranular. The mineralogy is Ca-plagioclase (40%), quartz (30%), hornblende (10%) and epidote (3%). Accessory minerals include zircon, apatite, and opaque minerals. Hornblende is dark-to-pale green coloured (Fig. 3c). There are fibrous amphiboles in contact with fine-grained quartz-feldspar granoblastic domains (Fig. 3d). The metamorphic peak assemblage includes hornblende and ternary feldspar (dark), a relic of the pre-mylonitic mineral assemblage (Fig. 3e). Quartz rarely shows lobate contacts against plagioclase due to high-temperature grain boundary migration, but the main deformation mechanism is bulging and recovery [1] (Fig. 3f). Hornblende presents zonation, epidote coronas and opaque inclusions.

1.2.4. Sample Mi30

Dark green layered migmatite injected by folded Kfs-rich granitic (leucosome) veins (coord.: x = 674723; y = 6198889). The layering (SL: 260/70) becomes partially into a mylonitic foliation, and the grain size is due to mylonitization (Fig. 4a). Leucosome veins are deformed (Fig. 4b). The main texture is granoblastic inequigranular (Fig. 4c). The mineralogy is composed of quartz (35%), Ca-plagioclase (saussurite) (35%), K-feldspar (albite, microcline) (25%), biotite (3%), epidote (0.5%), chlorite (0.2%) and sericite (0.5%). Accessory minerals are opaques, apatite, zircon, and allanite. Ca-plagioclase shows a myriad of sericite-epidote inclusions (Fig. 4d). There are two kinds of biotite: (i) oriented selvedge of pale-green biotite and (ii) brown biotite aggregates associated with the accessory minerals. Bulging and recovery are the mechanisms of grain-boundary migration recrystallisation in quartz. The allanite is in isolated grains and has at least 500 μm in size (Fig. 4e). Zircons usually are associated with sericite-epidote aggregates (Fig. 4f).

1.2.5. Sample Mi14

The primary rock is a medium-grained grey orthogneiss, crosscut by a K-feldspar-rich pegmatite (coord.: x=676057; y=6263943) (Fig. 5a). The texture of the grey orthogneiss is granoblastic inequigranular and lobate. The mineralogy contains plagioclase (An43) (45%), quartz (30%), K-feldspar (20%), and very few biotite. Accessory minerals are apatite, zircon, and muscovite.

1.2.6. Sample Mi19B

Composite-layered mylonitic granitoid (coord.: x=660189, y=6219998). The “granitic” layers produced a ribbon-quartz, Kfs-rich, porphyroclastic mylonite (Fig. 5b). The mylonitic granite crosscut a fine-grained granoblastic metapsammite and a lepidoblastic mica-schist with biotite muscovite and tourmaline. The mylonitic foliation (Sm: 330/26) was affected by upright cylindrical folding, whose axes parallel the stretching lineation (Lm: 20/195). The thin section reveals a fine-grained muscovite-rich quartz-feldspathic matrix, crosscut by 1-2 mm thick anastomosed quartz ribbons (Fig. 5c). Lobate quartz-grains in these ribbons are medium-grained, although

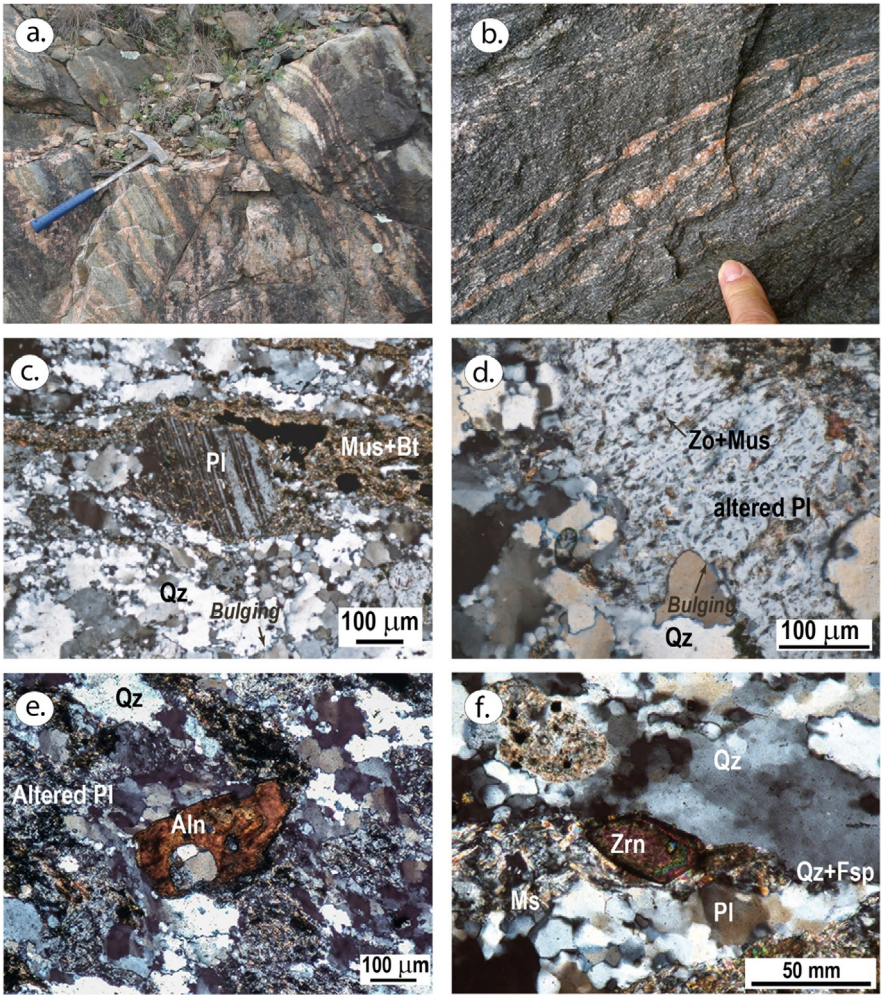

Fig. 3. Hbl-bearing orthogneisses (sample Mi21): a) Amphibole-bearing orthogneiss with pegmatite injections; b) incipient cataclastic deformation on the same outcrop; c) Hornblende associated with epidote and opaque minerals; d) Hbl-Pl-bearing gneiss (crossed Nicols); e) Older Ca-plagioclase surrounded by recrystallised matrix; f) Remnant of older quartz-boundary surrounded by low-temperature recrystallised matrix (crossed Nicols).

developing an incipient bulging and undulose extinction. The inequigranular matrix has a granoblastic polygonal texture, and the biotite is decussate (Fig. 5d). This matrix surrounds large plagioclase grains (An25). Muscovite is often secondary, but there are also large kinked muscovites. We also found biotite selvedges parallel to the layering.

1.3. Petrographic description of supplementary samples

1.3.1. Sample CNP122

Epidote-bearing tremolite schist represents a set of mafic rocks interspersed within the felsic orthogneisses of La China Complex (coord.: x=697392; y=6300113). In the field, they usually appear as amphibolite blocks or lenses (Fig. 5e). These mafic rocks have different degrees

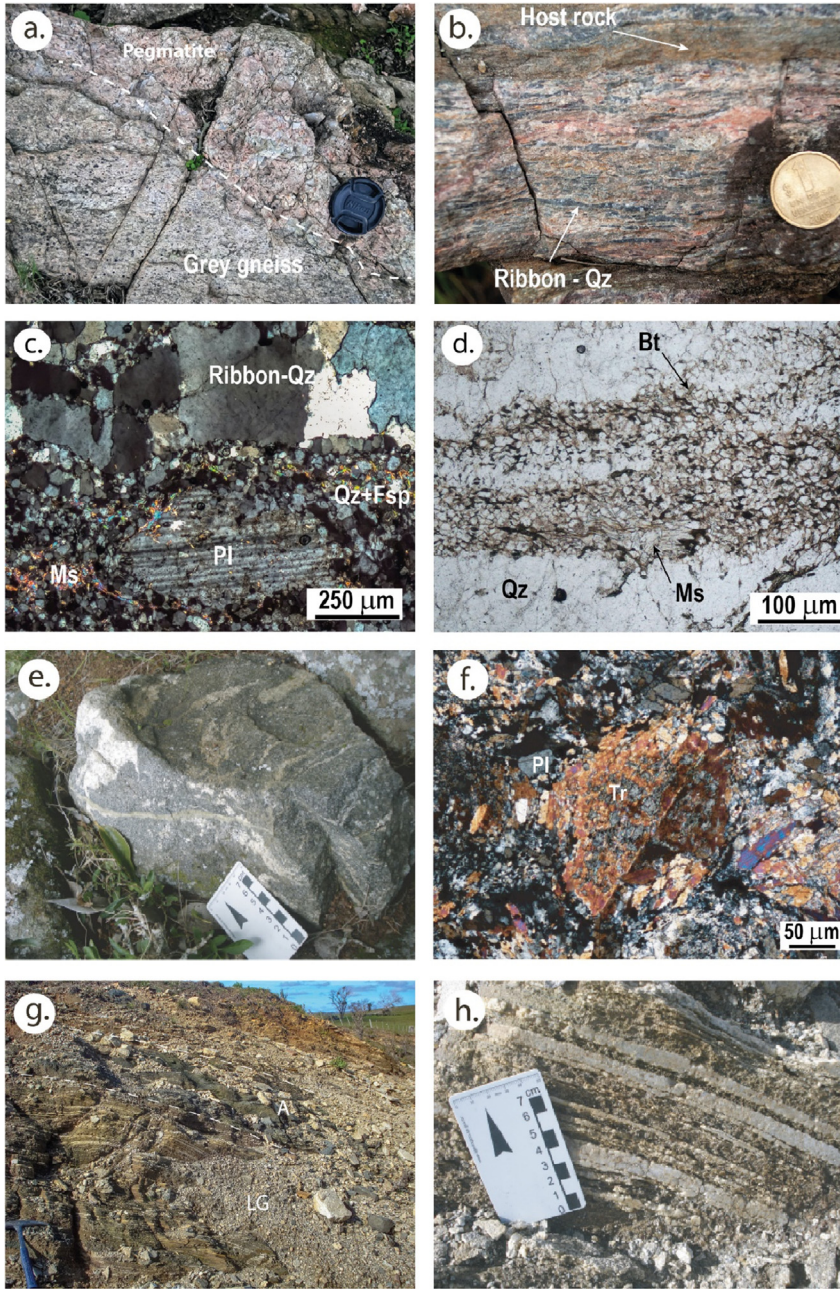

Fig. 4. Biotite-bearing migmatite orthogneiss (sample Mi30): a) Composite layered migmatite showing concordant granitic veins; b) Diffuse segregation of in-situ leucosome; c) main texture of the rock showing fine-grained Bt + Ms layers and plagioclase grains in a quartz-feldspathic matrix; d) Altered saussuritic plagioclase with epidote-sericite inclusions; e) Isolated crystal of allanite in a matrix with complete alteration of feldspar; f) Subhedral zircon in the quartz-feldspathic matrix.

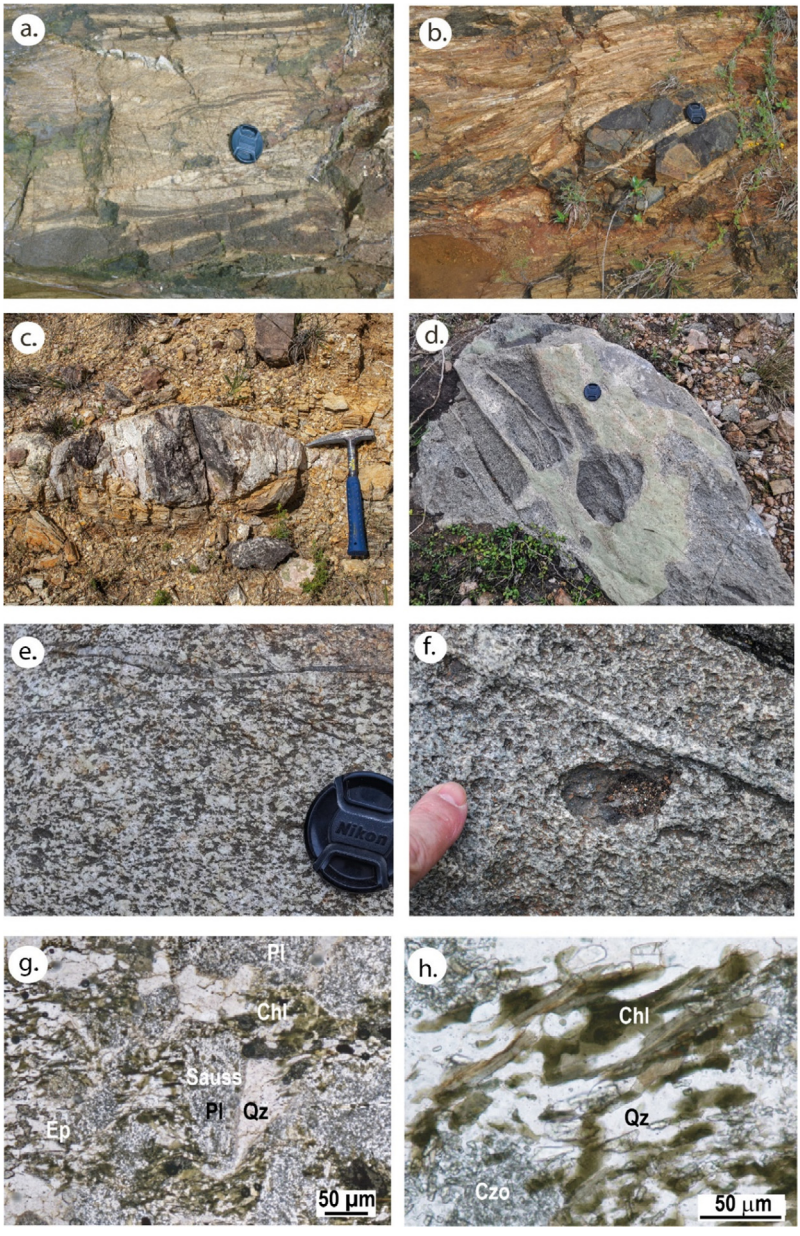

Fig. 5. Different orthogneisses and mafic rocks: a) Felsic orthogneiss crosscut by a K-feldspar pegmatite (Mi14); b) Mylonitic K-feldspar granitoid within biotite-tourmaline bearing schist (Mi19b); c) Detailed texture showing a folded ribbon-quartz (vein) crosscutting a quartz-feldspathic granoblastic matrix with decussate biotite and larger kinked muscovite (centre below; crossed Nicols); d) Idem, granoblastic matrix (natural light); e) Amphibolite boudin (CNP009); f) Twinned tremolite showing symplectite with Ab in retrograde mafic schist (CNP122); g) Low-angle cm-width gneissic banding (LG), showing the alternation between felsic layered gneisses and amphibolites (A)(CNP30A); h) Detail of gneiss layering.

of retrograde metamorphism. The symplectite between magnetite and tremolite represents the dominant texture. The tremolite texture is an aggregate of fibrous poikiloblastic bundles (> 2 mm). Basal sections show the trace of twins on (001) face (Fig. 5f). Some altered plagioclases (saussurite), quartz and opaques filled up the interstitial space among tremolite crystals.

1.3.2. Sample CNP30A

Straight layered fine-grained gneiss interspersed with amphibolite (coord. UTM84 21S: x = 698689; y = 6302989) (Fig. 5g). The mylonitic foliation (Sm: 70/27) is parallel to the centimetre-width layering (Fig. 5h) and contain a stretching lineation (Lm: 21/272). This banding represents the relicts of a wide high-strain zone with relative flat-lying foliation, which limited the Pavas and the Cerro Chato "terranes" (i.e., Sierra de Sosa high strain zone). The layering was produced at relatively high temperature and persisted despite many rocks in the region passed to retrograde conditions. Layered amphibolites are likely the same as those found in straight and short "boudins" or lenses but in the different structural setting. The thin section was unable here due to the alteration of the rock.

1.3.3. Sample CNP132

Fine-grained layered migmatitic gneiss containing biotite *schlieren* (Fig. 6a) (coord. UTM84 21S: x = 686153; y = 6263198). The gneissic layering (SL: 144/25) contains some amphibolite boudins unaffected by anatexis (Fig. 6b). Some white pegmatites are showing pinch-and-swell and crosscut the migmatitic gneiss (Fig. 6c). We select one pegmatite dyke for zircon sampling. Texture in quartz- feldspathic domains is granoblastic heterogranular with large patchy perthite K-feldspar. Muscovite is present as well as accessory minerals, e.g., zircon and apatite. The rock did not bring enough zircons of good quality (low common Pb) to produce an acceptable Pb-loss Discordia age.

1.3.4. Sample BT48

Medium grained gray granitoid crosscut by veinlets (Fig. 6d; coord. UTM wgs84 21S: x = 687409; y = 6280088). Mafic enclaves appear disseminated (Fig. 6f). The texture is granular hypidiomorphic and composed of poikilitic Ca-Plagioclase (saussurite) in the process of albitisation, microcline, quartz, chlorite, green biotite, zoisite, apatite, calcite, and sericite (Fig. 6g). Ca-plagioclase is subhedral and shows Ab and Carlsbad twins. Although the deformation is weak, the rock developed a domanial cleavage of its secondary hydrothermal mineralogy of chlorite and epidote (Fig. 6h). Fine-grained zoisite and sericite within plagioclase are alteration minerals. Hydrothermal albite is twinned and limpid. Brown biotite is magmatic and arranged around feldspar and quartz. Pressure shadows are often present around euhedral feldspar grains. Quartz texture is granoblastic and lobate.

1.3.5. Sample SY95A

Amphibole-biotite coarse-grained mesocratic granodiorite or monzogranite (coord. UTM wgs84 21S: x= 706825; y=6315572). The hand sample is a porphyroblastic orthogneiss (SL: 265/10; Lm: 10/238) (Fig. 7a). A mafic dyke crosscut the main granodiorite. The dyke transformed into a medium-grained amphibolite (D: 50/65) (Fig. 7b); there is a strong mineral lineation on it (Lm: 5/253) (Fig. 7c). The texture of the granodiorite is granular hypidiomorphic but slightly deformed. K-feldspar phenocrysts reach 3-4 cm and are surrounded by hornblende-biotite aggregates (Fig. 7d). The mineralogy is microcline, plagioclase, hornblende, quartz, biotite (brown), titanite (3%), apatite, opaque minerals, epidote, zircon, and monazite. Biotite and amphibole are intergrowing with titanite, apatite and monazite (Fig. 7e). The amphibolite shows a granoblastic texture composed of hornblende and plagioclase (Fig. 7f).

1.3.6. Sample Mi06

Low-angle composite mylonitic rock (SL: 085/20; Lm: 5/170) (Fig. 8a; coord.: x=699986; y=6285192). The outcrop comprises (i) a white augen gneiss and (ii) a fine-grained biotite mylonite. The protolith of the augen gneiss may be a pegmatite injected into the mylonite. Its

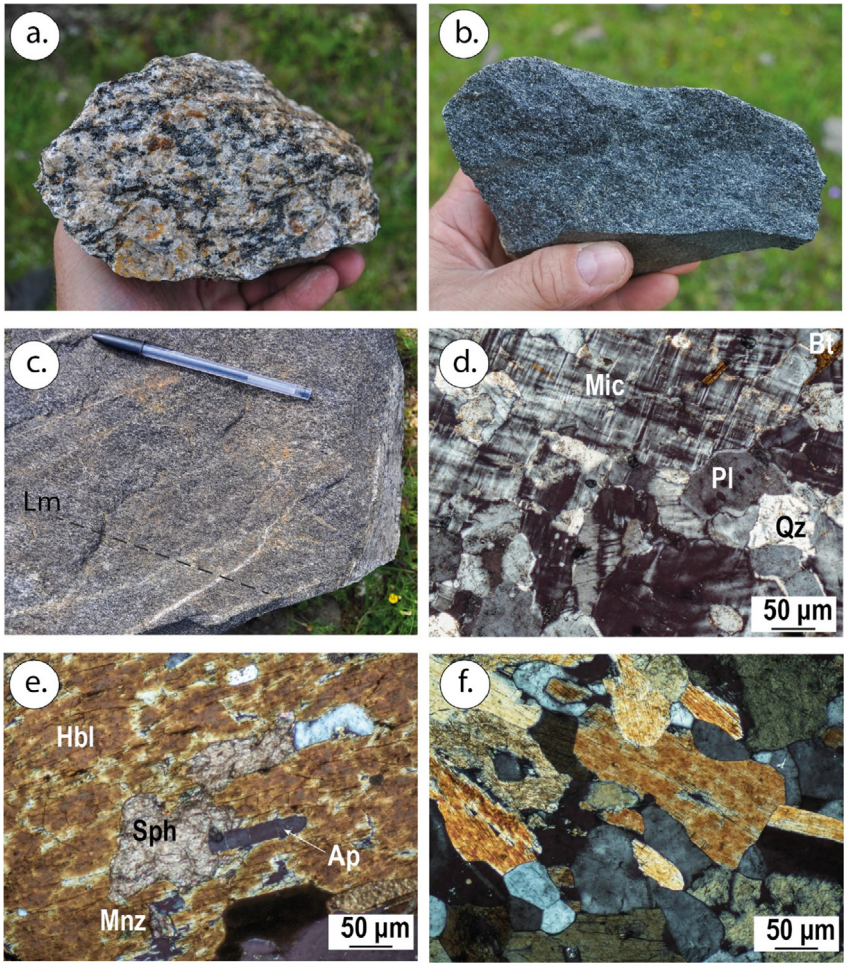

Fig. 6. a) Granitic gneiss with biotite schlieren (CNP132) (a to c) containing b) amphibolite boudins, c) "white" pegmatite dyke, concordant with the layering; d) Foliated grey orthogneiss (BT48) (d to g) with e) Magmatic texture observed in the field; f) Mafic enclaves; g) Domanial cleavage around saussuritic altered plagioclase (natural light). g) Chl-Ep bearing cleavage.

mineralogy includes K-feldspar, plagioclase (An50), quartz, muscovite, opaque minerals, biotite, apatite, and zircon. The mylonite has a fine-grained equigranular granoblastic texture. Its minerals are plagioclase, ternary feldspar, quartz, reddish biotite, apatite, and zircon. Porphyroclasts have a recrystallisation mantle (Fig. 8b). The pressure shadows show an aggregate of fine-grained feldspars (Fig. 8c, d). Porphyroclasts have an antiperthitic nucleus (Pl+Mic) (Fig. 8e, f). Recrystallisation could have occurred by rotation of subgrains within the augen themselves (Fig. 8g). Metamorphic plagioclase exhibits muscovite and quartz inclusions. Albite twins are fuzzy, irregular, and sinuous. Quartz appears in different forms: (i) black quartz fishes (Fig. 8c, d), (ii) ribbons (Fig. 8b, h) and (iii) equidimensional grains. Quartz ribbons and muscovite aggregates cover the porphyroclasts (Fig. 8i). Porphyroclasts define a blurred sigma-delta system, but the shear direction is ambiguous (Fig. 8a, b, f).

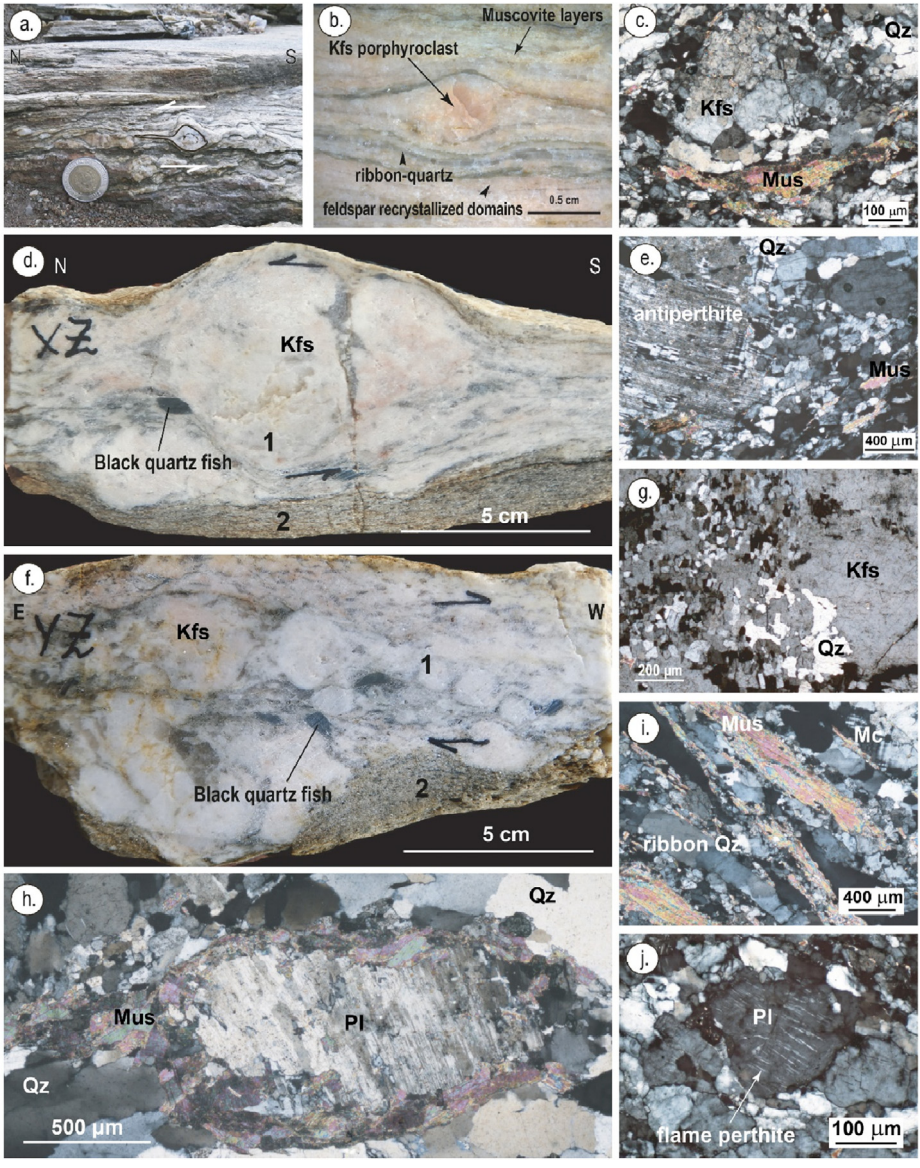

Fig. 7. a) Amphibole-biotite granodiorite (SY95) (a to f); b) medium-grained foliated amphibolite from a mafic dyke; c) stretching lineation of the amphibolite; d) texture of the granodiorite with recrystallised microcline phenocrysts, plagioclase, and quartz: e) Hbl containing titanite, apatite and monazite inclusions; f) granoblastic texture of the amphibolite (crossed Nicols).

2. U-Pb Isotopic Data of Zircons

The new U-Pb isotopic data by Laser ablation – ICP – MS are presented in Table I.

The correlation of different textural features between the sample's zircons is presented in Table II. Older U-Pb age references are presented in Table III.

Table I
LA-ICP-MS U-Pb zircon analytical data. The analytical errors are in the 1σ, but the selected spots for calculations at the 2σ error.

	RATIOS															AGES							
#	207Pb/ 235U	1 σ	206Pb/ 238U	1 σ	238U/ 206Pb	1 σ	207Pb/ 206Pb	1 σ	208Pb/ 206Pb	1 σ	Pb* (%)	Pb* ppm	Th ppm	U ppm	Th/U	T206/ 238	1σ	T207/ 235	1σ	T207/ 206	1σ	Conc.206/238 vs 207/206	Interpretation (Ma)
CNP13F - Layered amphibole – bearing orthogneiss																							
30.1	23.788	0.357	0.647	0.007	1.546	0.017	0.267	0.004	0.161	0.017	0.30	22.5	-	24.8	-	3216	27	3260	14	3287	24	97	Concordia Age: 3261 ± 16
34.1	22.683	0.601	0.649	0.008	1.540	0.018	0.253	0.007	0.201	0.027	0.26	55.3	22.5	58.1	**0.39**	3226	30	3213	26	3206	44	100	
25.1	23.742	0.372	0.651	0.007	1.536	0.017	0.264	0.004	0.233	0.034	0.11	18.7	16.9	18.9	**0.89**	3233	28	3258	14	3273	25	98	
26.1	22.969	0.579	0.652	0.013	1.534	0.031	0.256	0.007	0.255	0.047	0.71	6.2	-	7	-	3236	54	3226	31	3219	52	100	
12.1	24.380	0.471	0.652	0.006	1.534	0.015	0.271	0.006	0.122	0.006	0.41	45.9	-	50.2	-	3236	25	3284	19	3313	32	97	
35.1	23.808	0.511	0.655	0.005	1.527	0.013	0.264	0.006	0.166	0.004	0.34	41.5	35	46.6	**0.75**	3247	21	3261	21	3269	33	99	
27.1	23.361	0.378	0.658	0.008	1.521	0.018	0.258	0.004	0.207	0.022	0.22	12.8	7.5	13.4	**0.56**	3258	30	3242	15	3233	26	100	
2.1	23.631	0.447	0.662	0.006	1.512	0.013	0.259	0.005	0.201	0.020	0.21	50.9	-	52	-	3273	22	3253	18	3241	31	100	
1.1	24.378	0.435	0.662	0.006	1.511	0.013	0.267	0.005	0.159	0.005	0.15	66.3	13.8	68	**0.20**	3274	22	3284	17	3290	29	99	
3.1	24.879	0.420	0.668	0.005	1.497	0.012	0.270	0.005	0.190	0.010	0.18	70	12.8	72.9	**0.18**	3298	20	3304	17	3307	28	99	
36.1	23.481	0.543	0.669	0.007	1.496	0.015	0.255	0.006	0.135	0.014	0.16	29.1	19.2	30.7	**0.63**	3300	25	3247	24	3215	40	102	
6.1	25.327	0.479	0.676	0.007	1.479	0.014	0.272	0.006	0.134	0.006	0.17	44.6	13.3	45.3	**0.29**	3329	25	3321	19	3316	32	100	Concordia Age: 3339 ± 7.2
13.1	25.486	0.475	0.682	0.006	1.466	0.012	0.271	0.005	0.176	0.012	0.32	81.2	30.8	82.7	**0.37**	3353	21	3327	18	3312	28	101	
15.1	25.823	0.491	0.685	0.006	1.460	0.012	0.274	0.005	0.153	0.010	0.16	46.3	0.4	47.8	**0.01**	3363	22	3340	19	3326	30	101	
24.1	25.285	0.494	0.685	0.006	1.459	0.013	0.268	0.005	0.208	0.012	0.31	16.9	23.5	16.8	**1.40**	3365	24	3319	19	3292	31	102	
4.1	25.635	0.427	0.687	0.005	1.456	0.011	0.271	0.005	0.248	0.019	0.09	78.5	59.8	77.1	**0.78**	3370	20	3333	16	3310	27	101	
19.1	21.398	0.562	0.604	0.009	1.656	0.024	0.257	0.007	0.243	0.042	1.42	3.9	-	4.3	-	3045	35	3157	26	3229	46	94	
38.1	20.805	0.712	0.605	0.011	1.654	0.029	0.250	0.009	0.218	0.030	0.95	5.6	-	6.2	-	3048	42	3130	33	3182	59	95	
21.1	21.523	0.418	0.609	0.006	1.642	0.015	0.256	0.005	0.121	0.015	1.77	7.7	-	8.8	-	3067	23	3162	20	3224	32	95	
42.1	20.377	0.735	0.617	0.012	1.621	0.031	0.240	0.009	0.213	0.065	1.00	5.8	36.6	7.3	**5.05**	3098	47	3109	36	3117	64	99	
5.1	21.543	0.390	0.619	0.005	1.616	0.013	0.253	0.005	0.115	0.047	1.48	15	-	22	-	3105	20	3163	17	3200	29	97	
29.1	20.898	0.483	0.626	0.011	1.598	0.028	0.242	0.007	0.192	0.032	1.02	4.2	9.1	5.7	**1.59**	3134	45	3134	27	3134	48	99	
23.1	21.775	0.665	0.633	0.012	1.581	0.029	0.250	0.009	0.218	0.023	0.56	18.6	6.5	23.4	**0.28**	3160	47	3174	32	3183	56	99	
32.1	22.866	0.499	0.634	0.005	1.578	0.013	0.262	0.006	0.165	0.006	0.24	49.9	22.2	54	**0.41**	3165	21	3221	21	3257	33	97	
28.1	23.388	0.354	0.635	0.007	1.574	0.017	0.267	0.004	0.188	0.016	0.04	42.9	26.7	46.3	**0.58**	3170	27	3243	14	3289	24	96	
8.1	23.228	0.409	0.637	0.005	1.571	0.013	0.265	0.005	0.153	0.020	0.04	53.3	13	60.4	**0.22**	3176	21	3237	17	3275	29	96	
33.1	21.434	0.670	0.638	0.009	1.568	0.023	0.244	0.008	0.210	0.014	0.79	8.4	9.8	9.5	**1.03**	3180	35	3158	29	3145	48	101	
22.1	22.664	0.570	0.638	0.009	1.568	0.021	0.258	0.007	0.227	0.020	0.38	18.8	10.9	27.1	**0.40**	3180	33	3213	25	3233	43	98	
18.1	23.646	0.456	0.643	0.005	1.555	0.012	0.267	0.005	0.193	0.022	0.20	30.9	4	34.8	**0.12**	3201	19	3254	18	3287	29	97	
17.1	23.531	0.448	0.646	0.005	1.547	0.013	0.264	0.005	0.174	0.008	0.17	62	11.6	65.2	**0.18**	3214	20	3249	18	3271	28	98	
31.1	21.866	0.428	0.607	0.004	1.648	0.012	0.261	0.005	0.168	0.051	0.14	65	13.2	114	**0.12**	3058	18	3178	20	3254	32	93	
16.1	22.507	0.419	0.609	0.005	1.642	0.013	0.268	0.005	0.196	0.029	0.11	12.3	22.5	6.8	**3.31**	3066	19	3206	18	3295	28	93	
39.1	24.905	0.526	0.671	0.005	1.491	0.012	0.269	0.006	0.172	0.008	0.14	60.1	61.8	62.5	**0.99**	3308	21	3305	20	3302	32	100	
11.1	24.770	0.454	0.673	0.006	1.487	0.013	0.267	0.005	0.140	0.012	0.25	57.5	51.3	67.5	**0.76**	3316	23	3299	18	3289	30	100	
14.1	11.122	0.253	0.349	0.003	2.865	0.027	0.231	0.005	0.127	0.018	0.16	43.2	8.1	87.9	**0.09**	1930	15	2533	18	3060	31	63	
9.1	13.730	0.306	0.481	0.005	2.081	0.022	0.207	0.005	0.047	0.008	0.34	27.9	17.5	48.6	**0.36**	2529	23	2731	22	2884	42	87	
40.1	16.781	0.543	0.521	0.007	1.920	0.026	0.234	0.007	0.196	0.020	0.28	21.1	17.1	30.2	**0.57**	2703	29	2922	27	3077	47	87	
7.1	15.181	0.628	0.543	0.013	1.843	0.045	0.203	0.010	0.058	0.036	2.80	2.1	2.1	3.8	**0.56**	2795	55	2827	41	2850	84	98	

(*continued on next page*)

Table 1 (*continued*)

#	RATIOS										Pb* (%)	Pb* ppm	Th ppm	U ppm	Th/U	AGES							Conc.206/238 vs 207/206	Interpretation (Ma)
	207Pb/ 235U	1 σ	206Pb/ 238U	1 σ	238U/ 206Pb	1 σ	207Pb/ 206Pb	1 σ	208Pb/ 206Pb	1 σ						T206/ 238	1σ	T207/ 235	1σ	T207/ 206	1σ			
CNP13F - Layered amphibole – bearing orthogneiss																								
20.1	18.475	0.385	0.547	0.005	1.829	0.018	0.245	0.005	0.134	0.011	0.21	49.1	25.4	65.5	**0.39**	2812	22	3015	20	3153	34	89		
37.1	26.053	0.550	0.701	0.006	1.426	0.012	0.270	0.006	0.220	0.019	0.32	21.5	-	22.8	**-**	3425	22	3349	21	3303	33	103		
10.1	26.264	0.487	0.702	0.007	1.424	0.013	0.271	0.005	0.139	0.013	0.24	65.3	58.6	65.8	**0.89**	3429	25	3356	18	3314	31	103		
CNP77 - Augen Gneiss (muscovite-bearing mylonitic orthogneiss)																								
21.1	20.296	0.691	0.608	0.011	1.646	0.029	0.242	0.009	0.018	0.017	1.22	15	19.5	20	**0.98**	3060	43	3106	32	3135	61	97		Concordia Age: 3078 ± 30
24.1	18.297	0.467	0.610	0.007	1.639	0.019	0.218	0.006	0.056	0.024	2.19	12.9	-	17.9	**-**	3071	28	3006	26	2962	48	103		
1.1	19.519	0.406	0.613	0.006	1.630	0.015	0.231	0.005	0.018	0.006	0.46	39	56.1	53	**1.06**	3084	22	3068	20	3058	32	100		
6.1	18.933	0.644	0.615	0.012	1.625	0.031	0.223	0.008	0.151	0.063	0.37	20.7	28.2	25.7	**1.10**	3091	48	3038	33	3004	60	102		
27.1	20.255	0.380	0.623	0.005	1.605	0.012	0.236	0.004	0.006	0.005	3.70	55.3	23.2	75.1	**0.31**	3122	18	3104	18	3092	29	100		
16.1	24.435	0.503	0.667	0.006	1.500	0.012	0.266	0.006	0.201	0.019	0.05	43.1	-	44.1	**-**	3293	21	3286	20	3282	33	100		
10.1	23.869	0.608	0.675	0.009	1.482	0.021	0.257	0.007	0.286	0.023	0.57	14.5	-	13.9	**-**	3324	36	3263	25	3226	42	103		
20.1	25.306	0.516	0.675	0.005	1.482	0.012	0.272	0.006	0.235	0.014	0.00	73.7	23.1	75.4	**0.31**	3324	20	3320	20	3318	32	100		
3.1	24.398	0.516	0.675	0.006	1.481	0.014	0.262	0.006	0.108	0.045	0.10	64.8	58.7	68.6	**0.86**	3326	25	3284	20	3259	33	102		
23.1	17.125	0.522	0.591	0.008	1.692	0.024	0.210	0.007	0.087	0.018	0.79	7.6	30	11	**2.73**	2993	33	2942	29	2907	56	102		
9.1	17.392	0.807	0.592	0.018	1.689	0.050	0.213	0.012	0.065	0.044	0.50	3.4	-	6.1	**-**	2997	72	2957	47	2929	91	102		
26.1	17.275	0.286	0.576	0.004	1.736	0.011	0.218	0.004	0.067	0.011	0.05	53.3	30.8	65.8	**0.47**	2932	14	2950	17	2963	27	98		
29.1	18.365	0.340	0.598	0.004	1.672	0.012	0.223	0.004	0.017	0.008	0.00	27.8	48	38.7	**1.24**	3022	17	3009	18	3001	29	100		
34.1	1.583	0.113	0.167	0.003	5.994	0.097	0.069	0.006	0.310	0.017	1.69	11.5	21.1	49.5	**0.43**	995	15	964	44	894	160	111		
11.1	4.979	0.149	0.323	0.004	3.100	0.035	0.112	0.004	0.291	0.012	0.85	42.1	61.3	96.8	**0.63**	1803	18	1816	25	1831	59	98		
15.1	10.794	0.412	0.479	0.007	2.088	0.031	0.164	0.007	0.047	0.025	0.98	7.7	30.7	18	**1.71**	2523	30	2506	29	2492	56	101		
7.1	13.478	0.566	0.533	0.012	1.875	0.043	0.183	0.009	0.067	0.029	0.57	13.8	6.3	25.1	**0.25**	2756	50	2714	37	2683	72	102		
28.2	14.761	0.333	0.572	0.005	1.747	0.016	0.187	0.004	0.023	0.007	0.30	28.3	39.8	39.5	**1.01**	2917	22	2800	21	2717	38	107		
22.1	15.698	0.745	0.565	0.014	1.769	0.043	0.201	0.012	0.065	0.025	3.48	2.2	-	4.5	**-**	2889	58	2859	47	2837	99	101		
18.1	16.612	0.704	0.590	0.012	1.696	0.035	0.204	0.010	0.180	0.041	5.49	1.4	-	2.2	**-**	2987	49	2913	38	2862	78	104		Concordia Age: 3298±9
33.1	16.115	0.340	0.569	0.004	1.757	0.013	0.205	0.004	0.016	0.021	0.17	27.3	31.1	36	**0.86**	2905	17	2884	18	2869	29	101		
14.1	16.562	0.354	0.559	0.005	1.789	0.014	0.215	0.005	0.024	0.007	4.13	60.1	9.2	86.9	**0.11**	2862	19	2910	20	2943	35	97		
31.1	17.062	0.327	0.564	0.004	1.774	0.013	0.220	0.004	0.018	0.005	0.57	57.1	-	79.3	**-**	2882	17	2938	18	2977	31	96		
35.1	20.508	0.410	0.638	0.005	1.568	0.013	0.233	0.005	0.011	0.016	0.43	21.2	40.3	27	**1.49**	3181	20	3116	19	3074	31	103		Concordia Age: 2965±41
28.1	20.642	0.388	0.627	0.005	1.594	0.012	0.239	0.004	0.002	0.002	0.34	72.4	0.3	94.4	**0.00**	3140	18	3122	18	3111	28	100		
13.1	21.695	0.475	0.635	0.006	1.575	0.015	0.248	0.006	0.010	0.006	0.44	38.7	50.4	49.2	**1.03**	3170	24	3170	22	3170	38	99		
2.1	23.527	0.500	0.681	0.007	1.468	0.015	0.251	0.005	0.007	0.006	1.05	80	40.2	94.8	**0.43**	3349	26	3249	21	3188	34	105		
17.1	23.419	0.489	0.662	0.006	1.511	0.013	0.257	0.006	0.015	0.003	0.14	61.5	42	72.8	**0.58**	3275	21	3245	20	3226	34	101		
12.1	22.482	0.475	0.635	0.006	1.575	0.015	0.257	0.006	0.145	0.010	0.00	54.2	24.1	61.3	**0.39**	3168	24	3205	21	3228	34	98		
25.1	21.863	0.482	0.617	0.006	1.620	0.017	0.257	0.006	0.098	0.024	0.49	41.2	31.3	52.2	**0.60**	3099	25	3178	21	3228	35	95		
30.1	25.983	0.524	0.715	0.006	1.399	0.012	0.264	0.005	0.246	0.038	0.28	22.9	28.3	24.8	**1.14**	3476	22	3346	19	3269	30	106		
4.1	23.653	0.504	0.645	0.007	1.550	0.016	0.266	0.006	0.167	0.006	0.37	76	9.9	81.7	**0.12**	3210	25	3254	21	3282	34	97		
32.1	23.190	0.458	0.621	0.005	1.611	0.013	0.271	0.005	0.162	0.016	0.53	58.5	11.9	61.9	**0.19**	3113	21	3235	19	3312	30	93		
Mi21 – Amphibole – bearing orthogneiss																								
31.1	10.832	0.194	0.443	0.004	2.257	0.023	0.177	0.003	0.021	0.009	0.24	105.7	16.9	295	**0.06**	2365	0.02	2509	0.02	2628	0	89		UI: 2986±5
18.1	15.832	0.239	0.550	0.006	1.817	0.018	0.209	0.003	0.062	0.008	0.12	187.5	80.9	308	**0.26**	2826	0.02	2867	0.02	2895	0	97		
13.1	17.318	0.310	0.571	0.006	1.752	0.017	0.220	0.004	0.149	0.066	0.16	187.4	319	216	**1.48**	2911	0.02	2953	0.02	2981	0	97		
17.1	17.222	0.188	0.574	0.005	1.742	0.014	0.218	0.003	0.104	0.069	0.00	251	385	234	**1.64**	2925	0.02	2947	0.01	2962	0	98		

(*continued on next page*)

Table 1 (*continued*)

#	RATIOS										Pb* (%)	Pb* ppm	Th ppm	U ppm	Th/U	AGES							Conc.206/238 vs 207/206	Interpretation (Ma)
	207Pb/ 235U	1 σ	206Pb/ 238U	1 σ	238U/ 206Pb	1 σ	207Pb/ 206Pb	1 σ	208Pb/ 206Pb	1 σ						T206/ 238	1σ	T207/ 235	1σ	T207/ 206	1σ			
CNP13F - Layered amphibole – bearing orthogneiss																								
21.1	17.472	0.336	0.580	0.005	1.723	0.015	0.218	0.003	0.077	0.032	0.59	99.1	158	124	**1.27**	2951	0.02	2961	0.02	2968	0	99		
36.1	17.662	0.269	0.584	0.007	1.711	0.021	0.219	0.003	0.153	0.107	0.00	60.4	48.8	98.8	**0.49**	2966	0.03	2972	0.02	2975	0	99		
33.1	17.819	0.331	0.587	0.008	1.703	0.024	0.220	0.003	0.273	0.006	0.35	43.7	54.9	56.7	**0.97**	2979	0.03	2980	0.02	2981	0	99		
9.1	19.156	0.365	0.608	0.007	1.644	0.019	0.228	0.004	0.169	0.094	0.02	95	56.2	119	**0.47**	3063	0.03	3050	0.02	3041	0	100		
23.1	18.772	0.358	0.612	0.005	1.634	0.014	0.223	0.003	0.132	0.062	0.47	280.6	515	281	**1.83**	3077	0.02	3030	0.02	2999	0	102		LI: 1804 ± 17
15.1	19.094	0.282	0.612	0.006	1.633	0.016	0.226	0.003	0.104	0.038	0.00	66.3	49.3	79.9	**0.62**	3080	0.02	3047	0.02	3025	0	101		
1.1	19.973	0.514	0.616	0.010	1.624	0.025	0.235	0.004	0.178	0.004	0.04	73.7	67	92.8	**0.72**	3094	0.04	3090	0.02	3088	0	100		
5.1	19.645	0.476	0.617	0.009	1.622	0.024	0.231	0.003	0.178	0.004	0.01	76.6	85	119	**0.72**	3096	0.04	3074	0.02	3060	0	101		
19.1	19.308	0.277	0.621	0.006	1.612	0.016	0.226	0.003	0.137	0.065	0.04	157.3	58.3	201	**0.29**	3112	0.02	3057	0.02	3022	0	102		
10.1	20.085	0.420	0.622	0.008	1.607	0.021	0.234	0.005	0.225	0.009	0.00	50.9	53.1	62.3	**0.85**	3118	0.03	3095	0.02	3081	0	101		
7.1	20.622	0.575	0.632	0.011	1.582	0.027	0.237	0.004	0.133	0.020	0.04	68.8	69.2	86.6	**0.80**	3159	0.04	3121	0.03	3097	0	101		
4.1	20.251	0.499	0.639	0.009	1.566	0.023	0.230	0.003	0.191	0.005	0.10	109.4	127	147	**0.86**	3184	0.04	3103	0.02	3052	0	104		
Mi30 - Migmatite of Route 8 (quartz-feldspathic biotite gneiss with Kfs ad-situ veins)																								
18.1	7.722	0.175	0.382	0.006	2.621	0.038	0.147	0.003	0.019	0.007	0.00	79	17	124	**0.14**	2083	0.03	2199	0.02	2309	0.03	90		Concordia age: 3074 ± 7
16.1	16.386	0.298	0.550	0.007	1.817	0.024	0.216	0.004	0.038	0.001	0.30	160	45	255	**0.18**	2827	0.03	2900	0.02	2951	0.03	95		
10.1	16.718	0.349	0.559	0.009	1.790	0.028	0.217	0.003	0.087	0.008	0.12	57	14	85	**0.16**	2861	0.04	2919	0.02	2959	0.02	96		
21.1	16.333	0.273	0.562	0.008	1.781	0.025	0.211	0.003	0.012	0.004	0.00	170	13	236	**0.05**	2873	0.03	2896	0.02	2913	0.02	98		
32.1	17.012	0.364	0.568	0.009	1.762	0.027	0.217	0.003	0.090	0.002	0.02	103	60	157	**0.38**	2898	0.04	2935	0.02	2962	0.03	97		
19.1	17.513	0.320	0.577	0.008	1.732	0.023	0.220	0.004	0.021	0.003	0.05	95	12	145	**0.08**	2938	0.03	2963	0.02	2981	0.03	98		
26.1	17.417	0.317	0.578	0.008	1.731	0.025	0.219	0.003	0.096	0.006	0.00	219	108	306	**0.35**	2939	0.03	2958	0.02	2971	0.02	98		
31.1	17.923	0.387	0.585	0.009	1.709	0.026	0.222	0.003	0.171	0.010	1.08	140	135	155	**0.88**	2969	0.04	2986	0.02	2997	0.02	99		
9.1	18.075	0.368	0.597	0.009	1.674	0.024	0.219	0.003	0.155	0.025	2.37	116	92	168	**0.55**	3019	0.04	2994	0.02	2977	0.02	101		
15.1	18.483	0.344	0.601	0.008	1.665	0.022	0.223	0.004	0.192	0.002	0.00	268	294	299	**0.98**	3032	0.03	3015	0.02	3004	0.03	100		
17.1	18.912	0.347	0.601	0.008	1.665	0.022	0.228	0.004	0.159	0.007	0.01	109	92	147	**0.63**	3033	0.03	3037	0.02	3040	0.03	99		
36.1	19.144	0.348	0.603	0.009	1.659	0.026	0.230	0.003	0.097	0.007	0.00	147	92	186	**0.50**	3041	0.04	3049	0.02	3055	0.02	99		
25.1	18.181	0.320	0.604	0.009	1.657	0.024	0.219	0.003	0.108	0.031	0.02	165	98	226	**0.43**	3044	0.04	2999	0.02	2970	0.02	102		
13.1	18.530	0.363	0.605	0.009	1.653	0.024	0.222	0.003	0.097	0.008	1.74	242	119	266	**0.45**	3050	0.04	3018	0.02	2996	0.02	101		
33.1	19.208	0.412	0.605	0.009	1.652	0.026	0.230	0.004	0.121	0.010	0.19	118	83	155	**0.54**	3051	0.04	3052	0.02	3053	0.03	99		
27.1	19.203	0.370	0.608	0.010	1.645	0.026	0.229	0.003	0.112	0.008	0.00	143	107	182	**0.59**	3062	0.04	3052	0.02	3046	0.02	100		
5.1	19.306	0.290	0.609	0.007	1.641	0.020	0.230	0.004	0.094	0.009	0.22	99	40	135	**0.30**	3067	0.03	3057	0.01	3051	0.02	100		
2.2	18.960	0.285	0.610	0.008	1.640	0.020	0.226	0.003	0.093	0.001	0.19	167	104	231	**0.45**	3068	0.03	3040	0.01	3021	0.02	101		
28.1	19.170	0.361	0.610	0.010	1.640	0.027	0.228	0.003	0.113	0.005	0.25	88	39	124	**0.31**	3069	0.04	3050	0.02	3038	0.02	101		
30.1	18.412	0.388	0.610	0.009	1.639	0.025	0.219	0.003	0.067	0.024	0.05	216	123	309	**0.40**	3071	0.04	3011	0.02	2972	0.02	103		Concordia age: 1840±2
14.1	18.511	0.374	0.611	0.009	1.638	0.025	0.220	0.003	0.073	0.010	0.00	113	44	166	**0.27**	3072	0.04	3017	0.02	2980	0.03	103		
22.1	18.352	0.345	0.614	0.009	1.630	0.024	0.217	0.003	0.180	0.003	0.00	14	31	45	**0.68**	3084	0.04	3008	0.02	2958	0.02	104		
2.1	18.706	0.291	0.618	0.008	1.619	0.020	0.220	0.003	0.166	0.003	0.00	216	203	229	**0.89**	3100	0.03	3027	0.02	2978	0.02	104		

(*continued on next page*)

Table 1 (*continued*)

#	RATIOS										Pb* (%)	Pb* ppm	Th ppm	U ppm	Th/U	AGES						Conc.206/238 vs 207/206	Interpretation (Ma)
	207Pb/ 235U	1 σ	206Pb/ 238U	1 σ	238U/ 206Pb	1 σ	207Pb/ 206Pb	1 σ	208Pb/ 206Pb	1 σ						T206/ 238	1σ	T207/ 235	1σ	T207/ 206	1σ		
CNP13F - Layered amphibole – bearing orthogneiss																							
4.1	19.438	0.290	0.618	0.008	1.619	0.020	0.228	0.004	0.117	0.002	0.00	140	94	180	**0.52**	3101	0.03	3064	0.01	3040	0.02	101	
34.1	19.431	0.409	0.619	0.009	1.615	0.024	0.228	0.004	0.133	0.002	0.10	150	128	183	**0.70**	3107	0.04	3063	0.02	3035	0.02	102	
6.1	18.755	0.282	0.621	0.008	1.611	0.020	0.219	0.003	0.071	0.001	0.06	127	55	159	**0.35**	3113	0.03	3029	0.02	2974	0.02	104	
35.1	19.622	0.446	0.623	0.010	1.606	0.027	0.229	0.004	0.091	0.005	0.71	78	54	108	**0.50**	3120	0.04	3073	0.02	3042	0.03	102	
1.1	19.463	0.294	0.627	0.008	1.596	0.020	0.225	0.004	0.127	0.005	0.05	207	168	250	**0.67**	3136	0.03	3065	0.02	3019	0.03	103	
7.1	19.525	0.298	0.628	0.008	1.593	0.020	0.226	0.003	0.100	0.012	0.02	140	93	178	**0.52**	3140	0.03	3068	0.02	3021	0.02	103	
8.1	19.534	0.387	0.628	0.009	1.592	0.023	0.226	0.003	0.117	0.002	0.00	130	89	170	**0.52**	3142	0.04	3069	0.02	3021	0.02	103	
11.1	20.030	0.401	0.631	0.010	1.585	0.024	0.230	0.004	0.098	0.003	0.18	93	45	124	**0.36**	3153	0.04	3093	0.02	3054	0.03	103	
20.1	17.391	0.319	0.553	0.007	1.809	0.024	0.228	0.004	0.111	0.003	0.02	167	79	190	**0.41**	2837	0.03	2957	0.02	3039	0.03	93	
12.1	17.529	0.360	0.559	0.009	1.790	0.028	0.228	0.004	0.078	0.003	0.39	82	46.4	102	**0.45**	2862	0.04	2964	0.02	3035	0.02	94	
3.1	5.490	0.092	0.345	0.004	2.903	0.036	0.116	0.002	0.085	0.051	0.00	353	204	852	**0.24**	1908	0.02	1899	0.02	1889	0.02	100	UI: 1917±13 LI: 1037±146
16.1	5.581	0.104	0.348	0.005	2.878	0.037	0.117	0.002	0.067	0.001	0.14	162	92	425	**0.22**	1923	0.02	1913	0.02	1903	0.03	101	
15.1	5.691	0.098	0.351	0.004	2.852	0.034	0.118	0.002	0.063	0.010	0.00	184	92	494	**0.19**	1937	0.02	1930	0.02	1922	0.03	100	
35.1	5.753	0.103	0.350	0.004	2.854	0.032	0.119	0.002	0.046	0.001	0.04	235	87	548	**0.16**	1937	0.02	1939	0.02	1942	0.03	99	
6.1	6.030	0.108	0.361	0.005	2.774	0.036	0.121	0.002	0.098	0.004	0.00	109	78	268	**0.29**	1985	0.02	1980	0.02	1976	0.03	100	UI: 1986±18
22.1	5.959	0.092	0.365	0.004	2.744	0.032	0.119	0.002	0.109	0.088	0.00	364	174	809	**0.22**	2003	0.02	1970	0.01	1935	0.03	103	
7.1	6.100	0.108	0.365	0.005	2.740	0.034	0.121	0.002	0.093	0.002	0.03	144	85	348	**0.24**	2006	0.02	1990	0.02	1974	0.03	101	
34.1	6.115	0.110	0.367	0.004	2.728	0.031	0.121	0.002	0.087	0.006	0.00	184	137	438	**0.31**	2014	0.02	1992	0.02	1971	0.03	102	
5.1	6.184	0.110	0.368	0.005	2.720	0.034	0.122	0.002	0.110	0.002	0.24	104	69	239	**0.29**	2018	0.02	2002	0.02	1986	0.03	101	
24.1	6.055	0.093	0.368	0.004	2.714	0.032	0.119	0.002	0.082	0.020	0.15	182	214	413	**0.52**	2022	0.02	1984	0.01	1944	0.03	104	
1.1	12.929	0.221	0.485	0.006	2.064	0.026	0.194	0.003	0.031	0.002	0.25	405	96	725	**0.13**	2547	0.03	2674	0.02	2772	0.02	91	UI: 2973±15
14.1	14.778	0.291	0.532	0.007	1.880	0.026	0.202	0.003	0.055	0.005	0.00	76	38	96	**0.39**	2750	0.03	2801	0.02	2838	0.03	96	
4.1	16.598	0.303	0.573	0.008	1.746	0.023	0.210	0.003	0.078	0.004	0.75	169	61	204	**0.30**	2919	0.03	2912	0.02	2907	0.02	100	
30.1	17.422	0.323	0.593	0.007	1.686	0.021	0.213	0.004	0.056	0.002	0.00	238	81	305	**0.27**	3002	0.03	2958	0.02	2929	0.03	102	
2.1	18.908	0.332	0.630	0.008	1.588	0.021	0.218	0.003	0.109	0.010	0.00	172	116	222	**0.52**	3149	0.03	3037	0.02	2964	0.02	106	
29.1	17.649	0.259	0.577	0.007	1.733	0.020	0.222	0.003	0.073	0.016	0.52	88	59	161	**0.36**	2937	0.03	2971	0.01	2994	0.02	98	
8.1	18.409	0.339	0.597	0.008	1.675	0.023	0.224	0.003	0.124	0.029	0.03	211	217	241	**0.90**	3018	0.03	3011	0.02	3007	0.02	100	
31.1	18.374	0.358	0.594	0.007	1.683	0.020	0.224	0.004	0.080	0.005	0.27	35	13	76	**0.17**	3007	0.03	3010	0.02	3011	0.03	99	
26.1	19.170	0.286	0.620	0.007	1.612	0.018	0.224	0.003	0.096	0.012	0.13	199	134	241	**0.55**	3111	0.03	3050	0.01	3011	0.02	103	
19.1	4.876	0.088	0.313	0.004	3.194	0.040	0.113	0.002	0.039	0.008	0.58	96	69	176	**0.39**	1756	0.02	1798	0.02	1847	0.03	95	LI: 1887±28
12.1	6.170	0.123	0.374	0.005	2.677	0.037	0.120	0.002	0.086	0.004	0.12	89	59	204	**0.29**	2046	0.02	2000	0.02	1953	0.03	104	
28.1	6.165	0.087	0.372	0.004	2.692	0.026	0.120	0.002	0.096	0.003	1.31	103	104	330	**0.32**	2036	0.02	1999	0.01	1962	0.02	103	
33.1	6.526	0.123	0.390	0.005	2.563	0.030	0.121	0.002	0.063	0.001	0.00	267	141	624	**0.23**	2124	0.02	2049	0.02	1975	0.03	107	
25.1	5.878	0.095	0.344	0.004	2.905	0.032	0.124	0.002	0.087	0.006	1.45	98	80	205	**0.39**	1907	0.02	1958	0.01	2012	0.03	94	
23.1	9.642	0.245	0.507	0.006	1.971	0.024	0.138	0.004	0.046	0.005	0.34	473	149	684	**0.22**	2646	0.03	2401	0.02	2200	0.03	120	
11.1	7.400	0.142	0.385	0.005	2.596	0.034	0.139	0.002	0.048	0.005	0.10	233	94	379	**0.25**	2101	0.02	2161	0.02	2218	0.03	94	
36.1	12.043	0.210	0.509	0.006	1.967	0.022	0.172	0.003	0.031	0.002	0.00	105	20	158	**0.12**	2650	0.02	2608	0.02	2575	0.03	102	
17.1	13.098	0.261	0.451	0.006	2.220	0.030	0.211	0.003	0.040	0.003	0.06	206	47	245	**0.19**	2397	0.03	2687	0.02	2912	0.03	82	

(*continued on next page*)

Table 1 (*continued*)

#	RATIOS										Pb* (%)	Pb* ppm	Th ppm	U ppm	Th/U	AGES						Conc.206/238 vs 207/206	Interpretation (Ma)
	207Pb/ 235U	1 σ	206Pb/ 238U	1 σ	238U/ 206Pb	1 σ	207Pb/ 206Pb	1 σ	208Pb/ 206Pb	1 σ						T206/ 238	1σ	T207/ 235	1σ	T207/ 206	1σ		
CNP13F - Layered amphibole – bearing orthogneiss																							
Mi19B – Mylonitic metagranite																							
7.1	2.522	0.100	0.193	0.004	5.191	0.106	0.095	0.002	0.163	0.051	3.30	167	699	670	**1.04**	1136	0.01	1278	0.01	1527	0.02	74	UI: 1987±3.2
14.1	4.841	0.072	0.299	0.003	3.347	0.032	0.118	0.002	0.114	0.007	0.14	106	205	345	**0.60**	1685	0.01	1792	0.01	1919	0.02	87	
24.1	5.313	0.111	0.318	0.003	3.149	0.034	0.121	0.002	0.147	0.022	0.00	102	123	275	**0.45**	1778	0.01	1871	0.01	1.976	0.02	89	
18.1	5.393	0.068	0.329	0.003	3.040	0.023	0.119	0.002	0.152	0.033	1.88	100	145	262	**0.55**	1833	0.01	1884	0.01	1940	0.02	94	
12.1	5.390	0.080	0.329	0.004	3.037	0.035	0.119	0.002	0.111	0.011	0.00	110	98	288	**0.34**	1835	0.01	1883	0.01	1937	0.02	94	
34.1	5.506	0.097	0.332	0.004	3.016	0.034	0.120	0.002	0.198	0.016	0.63	93	200	222	**0.90**	1846	0.01	1902	0.01	1963	0.02	94	
6.1	5.446	0.085	0.332	0.004	3.013	0.032	0.119	0.002	0.095	0.029	0.00	122	93	287	**0.33**	1848	0.01	1892	0.01	1941	0.02	95	
21.1	5.635	0.121	0.339	0.004	2.952	0.033	0.121	0.002	0.120	0.017	0.39	126	268	371	**0.72**	1880	0.01	1921	0.01	1966	0.03	95	
9.1	5.768	0.091	0.341	0.004	2.931	0.035	0.123	0.002	0.181	0.009	0.22	91	203	215	**0.95**	1893	0.01	1942	0.01	1994	0.02	94	
2.1	5.600	0.081	0.341	0.003	2.929	0.029	0.119	0.002	0.110	0.007	0.73	98	122	277	**0.44**	1894	0.01	1916	0.01	1941	0.02	97	
13.1	5.811	0.090	0.344	0.004	2.911	0.035	0.123	0.002	0.129	0.009	0.05	108	140	271	**0.52**	1903	0.02	1948	0.01	1996	0.02	95	
26.1	5.884	0.132	0.347	0.004	2.880	0.032	0.123	0.002	0.101	0.016	0.40	80	89	188	**0.47**	1921	0.01	1959	0.01	1999	0.03	96	
36.1	5.874	0.107	0.352	0.003	2.844	0.028	0.121	0.002	0.129	0.018	0.11	142	188	377	**0.50**	1942	0.01	1957	0.01	1973	0.02	98	
20.1	6.180	0.094	0.359	0.004	2.782	0.028	0.125	0.002	0.105	0.016	0.13	82	121	246	**0.49**	1979	0.01	2002	0.01	2025	0.02	97	
11.1	6.139	0.083	0.361	0.004	2.774	0.027	0.124	0.002	0.121	0.035	0.34	103	4	183	**0.02**	1985	0.01	1996	0.01	2007	0.02	98	
1.1	6.107	0.089	0.363	0.004	2.758	0.028	0.122	0.002	0.110	0.002	0.11	90	82	212	**0.39**	1994	0.01	1991	0.01	1988	0.02	100	
27.1	6.246	0.132	0.363	0.004	2.757	0.031	0.125	0.002	0.196	0.023	0.89	125	366	460	**0.80**	1995	0.01	2011	0.01	2028	0.03	98	LI: 783±18
30.1	6.215	0.104	0.369	0.004	2.709	0.030	0.122	0.002	0.113	0.009	0.00	93	78	217	**0.36**	2025	0.02	2007	0.01	1987	0.02	101	
28.1	6.374	0.104	0.369	0.004	2.708	0.029	0.125	0.002	0.142	0.038	0.73	62	194	149	**1.31**	2026	0.01	2029	0.01	2031	0.02	99	
33.1	6.312	0.105	0.370	0.004	2.701	0.030	0.124	0.002	0.134	0.007	0.00	102	155	247	**0.63**	2030	0.02	2020	0.01	2010	0.02	101	
16.1	6.294	0.095	0.371	0.004	2.696	0.026	0.123	0.002	0.141	0.015	0.19	123	124	311	**0.40**	2034	0.01	2018	0.01	2001	0.02	101	
32.1	6.379	0.111	0.372	0.004	2.690	0.031	0.124	0.002	0.243	0.020	0.08	103	244	232	**1.05**	2038	0.02	2029	0.01	2021	0.02	100	
25.1	6.451	0.140	0.374	0.004	2.674	0.029	0.125	0.002	0.140	0.054	0.60	74	205	165	**1.24**	2048	0.01	2039	0.01	2031	0.03	100	
35.1	6.551	0.132	0.376	0.004	2.661	0.028	0.126	0.002	0.132	0.055	0.00	71	30	165	**0.18**	2057	0.01	2053	0.01	2049	0.03	100	
5.1	6.360	0.089	0.378	0.004	2.644	0.026	0.122	0.002	0.107	0.005	0.59	101	98	287	**0.34**	2068	0.01	2027	0.01	1985	0.02	104	
22.1	6.413	0.137	0.379	0.004	2.640	0.029	0.123	0.002	0.131	0.024	0.25	43	67	138	**0.49**	2071	0.02	2034	0.01	1997	0.03	103	
19.1	6.496	0.097	0.380	0.004	2.635	0.025	0.124	0.002	0.108	0.009	0.21	94	96	219	**0.44**	2074	0.01	2045	0.01	2017	0.02	102	
8.1	6.536	0.100	0.380	0.005	2.631	0.031	0.125	0.002	0.108	0.005	0.11	72	62	183	**0.34**	2077	0.02	2051	0.01	2025	0.02	102	
15.1	6.524	0.100	0.382	0.004	2.621	0.026	0.124	0.002	0.138	0.014	0.00	122	133	281	**0.47**	2084	0.01	2049	0.01	2015	0.02	103	
31.1	6.533	0.107	0.382	0.004	2.615	0.029	0.124	0.002	0.109	0.016	0.00	72	83	179	**0.47**	2088	0.02	2050	0.01	2013	0.02	103	
10.1	6.570	0.102	0.383	0.005	2.611	0.031	0.124	0.002	0.097	0.002	0.08	118	102	289	**0.35**	2090	0.02	2055	0.01	2020	0.02	103	
3.1	6.690	0.092	0.393	0.004	2.545	0.024	0.124	0.002	0.199	0.003	0.21	97	173	222	**0.78**	2136	0.01	2071	0.01	2007	0.02	106	
4.1	6.813	0.091	0.396	0.004	2.527	0.024	0.125	0.002	0.117	0.033	1.44	101	150	280	**0.54**	2149	0.01	2087	0.01	2027	0.02	106	

Table II
Textural features of zircon grains from the studied samples and interpretation.

sample	External shape	Core texture	Main core texture	Recrystallisation/ Replacement	Overgrowth	Transgressive fronts and patches	Fractures and inclusions	Metamictization (%)	Ages	Th / U
CNP13F	Elongated (5:1), pale brown, round to subhedral	Patchy, convolute, non-luminescent; inner dark CL seam; outer bright CL seam	Highly resorbed, dark-CL; blurred "ghost" OZP; pyramidal sections w/ sector zoning	Broadening of oscillatory bands; darkening of wider bands	Homogeneous medium grey CL	Convolute/patchy cores, void infilling; round CL-bright unzoned patches	Healed fractures	30% of zircons (black cauliflower)	Core: 3.3 Ga; rim: 2.8 Ga	Overdispersed
CNP77	Stubby (2:1) and round, rough surface, fractured (subhedral); zircon mixture	Inherited resorbed patchy dark inner cores (25%)	1. broadened OZP zoning. 2. bright cloudy crystallisation	Dark overgrowth. Transgressive fuzzy zoned or unzoned recrystallisation	Dark-CL fuzzy sector zoning pattern; planar growth banding	Highly resorbed convolute pattern, void in-filling, transgressive fronts	Very fractured; Non-luminescent healed-fractures (50%)	Non-luminescent cataclastic elongated zircons (40%); cauliflowers (10%)	Core1: 3.3-3.0 Ga; rim1: 2.7 Ga; core2: 2.0-1.8 Ga; rim2?	Overdispersed 2 trends (< 0.1)
Mi21	Subhedral to anhedral (round) (2:1), smooth surface; very fractured	Core 1: Inherited dark CL OZP and internal transgressive bulging; completely resorbed non-luminescent roots.	Core 2: Original euhedral medium-grey CL oscillatory pattern zoning.	Broadening of OZP; dark CL thickened sectors: some overgrowth controlled by healed fractures	Planar / convolute growth banding; fir-tree and radial sector zoning patterns	CL-bright transgressive fronts through "ghost" OZP (internal and outer cores)	Fractured; healed-fractures and composite zircons	Not observed	Core 2: 3.1 Ga; CL- bright unzoned growth rim: 2.2 Ga	Overdispersed
Mi30	Subhedral (round); aspect ratio 2:1; rough borders; fractured	The CL-dark homogeneous inner core	Original euhedral OZP (core 2) affected by sector zoning recrystallisation (60%), broadened in the centre.	Bright luminescent overgrowth (transgressive over inherited structures)	Transgressive planar growth banding (dominant); fir-tree sector zoning new overgrowth	Transgressive fronts affecting the sector zoning	Recrystallisation after fracturing; healed-fractures	Very few non -luminescent inner cores (metamict)	Core 2: 3.0 Ga; sector zoning: 1.9 Ga? 2.outer rim: 1.77 Ga	Magmatic (0.1 - 1.0)
Mi14	Euhedral. Aspect ratio 3:1; mostly fractured; very rough borders; annealed metamict	CL-dark patchy or convolute inner core (20%) very resorbed	Almost totally annealed (polygonal) zircon; some preserve OZP but broaden; Smooth core surface; distinct core and rim	Planar sector zoning recrystallisation	New growth zone: dark CL homogeneous	Hydrothermal recrystallisation; leaching fluids	Healed fractures; altered fractures (metamict infilling)	Abundant in the inner cores	Core: 2.95 Ga; sector zoning + annealing: 2.0 Ga	2 trends (0.1-1.0) - (0.2-0.4)
Mi19B	Subhedral to round; aspect ratio 2:1	Inherited magmatic zircons (2.04 Ga)	a blurred magmatic broadening of bands.	Sector zoning recrystallisation.	Medium-grey CL planar zoning.	CL-bright concordant front.	α-decay damage cracks	Material loss on fractures	Inherited: 2.0 Ga; sector zoning: 46 ± 44 Ma	1 trend (0.4-1.0)

Table III
Supplementary database of U-Pb geochronological results for the Nico Pérez Terrane (including the Rivera block).

#	sample	Latitude	Longitude	Age (Ma)	2σ	Rock-type	Unit	Method	Interpretation	Reference
1	27-G-35	34°32'S	55°15"W	630	n.d.	phyllite	Lavalleja Group	U–Pb rutile	metamorphic	Sánchez-Bettucci et al. [6]
2	6198	34°21'04"S	55°07'43"W	1735	+32/-17	gneiss	Campanero Complex	U–Pb conv zircon	magmatic	Sánchez-Bettucci et al. [6]
3	8-9	33°30'39.10"S	55°12'2.51"W	1760	32	Rapakivi granite	Illescas Granite	Rb–Sr (WR) isochrone	magmatic	Umpierre & Halpern (1971)
4	AA-12	33°13'34.13"S	55°31'29,15"W	602	4.3	granitic mylonite	Sarandí del Yí Shear Zone	U-Pb LA-ICP-MS titanite	cooling age	Oriolo et al. (2016b)
5	AA-13	33°16'11.16"S	55°33'51.56"W	588	7.1	granitic mylonite	Sarandí del Yí Shear Zone	U-Pb LA-ICP-MS titanite	cooling age	Oriolo et al. (2016b)
6	AC-104 (cores)	34°17'36.37"S	54°25'5.57"W	778	7	Mafic migmatite	Cerro Olivo Complex	U-Pb SHRIMP zircon	magmatic	Masquelin et al. [7]
7	AC-104 (rims)	34°17'36.37"S	54°25'5.57"W	637	11	Mafic migmatite	Cerro Olivo Complex	U-Pb SHRIMP zircon	metamorphic	Masquelin et al. [7]
8	AC-133b	34°20'14.08"S	54°25'38.66"W	794	8	Felsic orthogneiss	Cerro Olivo Complex	U–Pb SHRIMP zircon	magmatic	Lenz et al. [8]
9	AC-137b (cores)	34°19'34.29"S	54°25'9.44"W	793	4	Tonalitic gneiss	Cerro Olivo Complex	U–Pb SHRIMP zircon	magmatic	Lenz et al. [8]
10	AC-137b (rims)	34°19'34.29"S	54°25'9.44"W	670	12	Tonalitic gneiss	Cerro Olivo Complex	U–Pb SHRIMP zircon	metamorphic	Lenz et al. [8]
11	AC-166	34°21'17.00"S	54°26'57.41"O	546	7	Porphyritic granite	El Pintor Granite	U-Pb ID TIMS	magmatic	Masquelin [9]
12	AC-167 (cores)	34°16'42.3"S	54°23'46.6"W	990	-	Kfs-augen migmatite	Cerro Olivo Complex	U-Pb SHRIMP zircon	inherited	Masquelin et al. [7]
13	AC-296m (cores)	34°18'54.24"S	54°23'53.72"W	796	8	Mafic granulite	Cerro Olivo Complex	U–Pb SHRIMP zircon	magmatic	Lenz et al. [8]
14	AC-296m (rims)	34°18'54.24"S	54°23'53.72"W	649	4	Mafic granulite	Cerro Olivo Complex	U–Pb SHRIMP zircon	metamorphic	Lenz et al. [8]
15	AC-301	34°20'42.2"S	54°23'56.1"W	626	25	Felsic migmatite	Cerro Olivo Complex	U-Pb SHRIMP zircon	metamorphic	Masquelin et al. [7]
16	AC-338a	34°18'23.80"S	54°24'25.87"W	802	12	Tonalitic gneiss	Cerro Olivo Complex	U–Pb SHRIMP zircon	magmatic	Lenz et al. [8]
17	AC-370a	34°24'5.13"S	54°24'33"W	780	5	Felsic migmatite	Cerro Olivo Complex	U–Pb SHRIMP zircon	magmatic	Lenz et al. [8]
18	AC-373b	34°20'29.80"S	54°24'3.35"W	795	8	Mafic granulite	Cerro Olivo Complex	U–Pb SHRIMP zircon	magmatic	Lenz et al. [8]
19	BRAF-212	34°27'47.66"S	55°10'3.68"W	1429	21	Rhyolite	Zanja del Tigre Complex	U-Pb ID-TIMS zircon	magmatic	Oyhantçabal et al. (2005)
20	BRAF-213	34°28'59.27"S	55°12'39.17"W	1492	4	Metagabbro	Zanja del Tigre Complex	U-Pb ID-TIMS zircon	magmatic	Oyhantçabal et al. (2005)
21	BUY-54-11	31°38'11.11"S	55°22'5.41"W	2095	15	Mafic granulite	Valentines– Rivera Granulitic Complex	U–Pb LA-ICP-MS zircon	magmatic	Oriolo et al. (2016a)
22	BUY-57-11 (cores)	31°41'18.30"S	55°16'13.60"W	2087	7	Tonalitic gneiss	Valentines– Rivera Granulitic Complex	U–Pb LA-ICP-MS zircon	magmatic	Oriolo et al. (2016a)
23	BUY-57-11 (rims)	31°41'18.30"S	55°16'13.60"W	1857	45	Tonalitic gneiss	Valentines-Rivera Granulitic Complex	U–Pb LA-ICP-MS zircon	metamorphic	Oriolo et al. (2016a)
24	BUY-61-11	31°44'52.40"S	54°56'51.46"W	2069	16	Leucocratic gneiss	Valentines– Rivera Granulitic Complex	U–Pb LA-ICP-MS zircon	magmatic	Oriolo et al. (2016a)
25	BUY-63-11	31°39'12"S	54°54'11"W	596	2	Amarillo Granite	Neoproterozoic granitoids	U–Pb LA-ICP-MS zircon	magmatic	Oriolo et al. (2016a)
26	BUY-64-11	32°53'40.18"S	54°48'58.26"W	598	2.2	granitic mylonite	Sierra de Sosa Shear Zone	Ar–Ar hornblende	cooling age	Oriolo et al. (2016a)
27	BUY-65-11	33°2'4.35"S	55°3'53.82"W	2106	21	Felsic granulite	Cerro Chato block	U–Pb LA-ICP-MS zircon	magmatic	Oriolo et al. (2016a)
28	BUY-66-11	32°50'40.69"S	54°44'7.47"W	549	2.9	granitic mylonite	Tupambaé Shear Zone	U–Pb LA-ICP-MS zircon	deformation	Oriolo et al. (2016b)
29	BUY-77-11	33°30'28"S	54°56'45"W	610	2	Zapicán diorite	Neoproterozoic granitoids	U–Pb LA-ICP-MS zircon	magmatic	Oriolo et al. (2016ab)
30	BUY-88-11	33°57'37.90"S	55°38'50.37"W	2078	4.7	granite	Cerro Colorado Granite	U–Pb LA-ICP-MS zircon	magmatic	Oriolo et al. (2016b)
31	CH-174	34°14'35.57"S	54°16'59.87"W	786	9	Felsic orthogneiss	Cerro Bori Orthogneisses	U–Pb SHRIMP zircon	magmatic	Lenz et al. [8]
32	CH-33a	34°17'19.72"S	54°11'4.51"W	767	9	Mafic granulite	Chafalote Paragneisses	U–Pb SHRIMP zircon	magmatic	Lenz et al. [8]
33	CH-43d	34°17'40.27"S	54°10'55.11"W	772-765?	-	Mafic granulite	Chafalote Paragneisses	U–Pb SHRIMP zircon	magmatic	Lenz et al. [8]
34	COR-42	34°24'42.40"S	54°25'11.56"W	797	8	Mylonitic orthogneiss	Cerro Bori Orthogneisses	U–Pb SHRIMP zircon	magmatic	Lenz et al. [8]
35	EP-210 (prov 3)	32°32'18.38"S	53°48'3.67"W	1823-665	-	psamo-pelitic schist	La Micaela Schists	U–Pb LA-ICP-MS zircon	detrital	Peel et al. [10]
36	EP-214 (prov 1)	32°33'11.32"S	53°48'37.31"W	587.7	3.9	Grt-chlorite schist	La Micaela Schists	U–Pb LA-ICP-MS zircon	detrital	Peel et al. [10]
37	EP-214 (prov 2)	32°33'11.32"S	53°48'37.31"W	569.5	3.3	Grt-chlorite schist	La Micaela Schists	U–Pb LA-ICP-MS zircon	detrital	Peel et al. [10]
38	EP-228 (cores)	32°35'38.42"S	53°49'44.17"W	753.8	8.4	anatectic paragneiss	Cerro Olivo Complex	U–Pb LA-ICP-MS zircon	detrital	Peel et al. [10]
39	EP-228 (rims)	32°35'38.42"S	53°49'44.17"W	668	17	anatectic paragneiss	Cerro Olivo Complex	U–Pb LA-ICP-MS zircon	metamorphic	Peel et al. [10]
40	FZ6	33°55'19.6"S	54°48'59.8"W	2787	6	Granitic mylonite	Archean granitoids	U-Pb LA-ICP-MS zircon	magmatic	Gaucher et al. (2014)
41	G	34°26'17.39"S	55°12'38.59"W	1203	65	Metagabbro	Cañada del Espinillo	K-Ar (WR)	cooling age	Gomez Rifas [11]

(*continued on next page*)

Table III (*continued*)

#	sample	Latitude	Longitude	Age (Ma)	2σ	Rock-type	Unit	Method	Interpretation	Reference
42	Hart1	34°25′19"S	54°14′25"W	762	8	gneiss	Cerro Olivo Complex	U–Pb SHRIMP zircon	magmatic	Hartmann et al. (2002)
43	Hart2	34°07'S	55°12′17"W	633	8	monzogranite	Santa Lucía Granite	U–Pb SHRIMP zircon	magmatic	Hartmann et al. (2002)
44	Hart3	34°16'S	54°07'W	571	8	dacite	Sierra de Aguirre Fm	U–Pb SHRIMP zircon	magmatic	Hartmann et al. (2002)
45	LAN-108	34°42′28"S	55°15′48.3"O	1433	6	Metatuffs	Parque UTE Group	U–Pb LA-ICP-MS zircon	magmatic	Gaucher et al. (2011)
46	MAZ-59	33°49′24.64"S	55°11′55.21"W	610	3	Granodiorite	Neoproterozoic granitoids	U–Pb LA-ICP-MS zircon	magmatic	Gaucher et al. (2014)
47	NP-154	34°35'51"S	55°09'23"W	1754	7	Mylonitic granite	Campanero Unit	U–Pb SHRIMP zircon	magmatic	Mallmann et al. (2007)
48	PCH-0869	34°20′21.39"S	54°24′17.74"W	788	6	Mafic granulite	Cerro Bori Orthogneisses	U–Pb SHRIMP zircon	magmatic	Lenz et al. [8]
49	SA-1	34°49′20"S	55°14′49"W	579	1.5	syenite	Pan de Azúcar Syenite	Ar-Ar hornblende	cooling age	Oyhantçabal et al. [12]
50	sample 1 (core)	33°32′15.90"S	54°55′37.45"W	3404	8	Metatonalite	La China Complex	U–Pb SHRIMP zircon	inherited	Hartmann et al. (2001)
51	sample 1 (rim)	33°32′15.90"S	54°55′37.45"W	2721	7	Metatonalite	La China Complex	U–Pb SHRIMP zircon	metamorphic	Hartmann et al. (2001)
52	sample 3 (core)	31°43′3.90"S	55°22′30.51"W	2140	6	Meta-trondhjemite	Rivera Granulitic Complex	U–Pb SHRIMP zircon	magmatic	Santos et al. (2003)
53	sample 3 (rim)	31°43′3.90"S	55°22′30.51"W	2077	6	Meta-trondhjemite	Rivera Granulitic Complex	U–Pb SHRIMP zircon	metamorphic	Santos et al. (2003)
54	sample 4 (core)	33°14′59"S	55°13′29"W	2163	22	Granulite	Valentines Granulitic Complex	U–Pb SHRIMP zircon	magmatic	Santos et al. (2003)
55	sample 4 (rim)	33°14′59"S	55°13′29"W	2058	3	Granulite	Valentines Granulitic Complex	U–Pb SHRIMP zircon	metamorphic	Santos et al. (2003)
56	SB-050	34°50'35"S	54°56'58"W	564	7	granite	Maldonado Granite	U–Pb SHRIMP zircon	magmatic	Oyhantcabal et al. (2009)
57	SB-632	34°35'24"S	55°26'30"W	584	13	granite	Mataojo granitic complex	Pb–Pb titanite	magmatic	Oyhantcabal et al. (2007)
58	SH-5	34°31'12"S	55°09'44"W	627	23	granodiorite	Neoproterozoic granitoids	U–Pb SHRIMP zircon	magmatic	Oyhantcabal et al. (2009)
59	SOL-3	34°01'44"S	55°08'W	583	7	monzogranite	Mangacha Granite	U–Pb SIMS zircon	magmatic	Gaucher et al. (2008)
60	U13MH04	33°15′12.13"S	54°43′44.45"W	600.4	1.1	quartz-micaschists	Las Tetas Complex	Ar-Ar muscovite	metamorphic	Oriolo et al. (2016b)
61	U13MH04	33°15′12.13"S	54°43′44.45"W	590	11	quartz-micaschists	Las Tetas Complex	Rb-Sr mica + WR isochrone	cooling age	Oriolo et al. (2016b)
62	URPR-12	34°37'S	54°51'W	587	16	granite	Aiguá Granite	U–Pb zircon	magmatic	Basei et al. (2000)
63	URPR-4a	34°34'S	55°10'W	572	14	granite	Carapé Granite	U–Pb conv zircon	magmatic	Sánchez-Bettucci et al. (2003)
64	URPR-63	34°54'14"S	55°14'13"W	1737	5.7	gneiss	Campanero Complex	U–Pb SHRIMP zircon	magmatic	Oyhantcabal et al. (2005)
65	URPR-68	34°29′58.34"S	55°13′1.45"W	3197-702	-	Metasandstone	Fuente del Puma Fm	U-Pb SHRIMP zircon	detrital	Oyhantcabal et al. (2005)
66	URPR-69	34°33′12.60"S	55° 5′26.66"W	3350-1780	-	Metasandstone	Zanja del Tigre Complex	U-Pb SHRIMP zircon	detrital	Oyhantcabal et al. (2005)
67	UY08-1	31°45′13.65"S	55°11′24.92"W	586	2.7	syenogranite	Las Flores Granite	U–Pb SHRIMP zircon	magmatic	Oyhantçabal et al. (2012)
68	UY08-2	31°32′38.65"S	55°29′43.93"W	585	2.5	syenogranite	Sobresaliente Granite	U–Pb SHRIMP zircon	magmatic	Oyhantçabal et al. (2012)
69	UY08-4a	31°39′50"S	55°10′17"W	1920	18	Mesocratic gneiss	Rivera Granulitic Complex	Th–U–Pb CHIME-EPMA mon	metamorphic	Oyhantçabal et al. (2012)
70	UY08-4a	31°39′50"S	55°10′17"W	606	10	Mylonite	Rivera Shear Zone	K–Ar muscovite	cooling age	Oyhantçabal et al. (2012)
71	UY08-5	31°41′29.69"S	55°22′59.03"W	1975	5	Leucocratic gneiss	Rivera Granulitic Complex	Th–U–Pb CHIME-EPMA mon	metamorphic	Oyhantçabal et al. (2012)
72	UY08-8	31°34′35.67"S	55°34′11.76"W	1981	2	Mesocratic gneiss	Rivera Granulitic Complex	Th–U–Pb CHIME-EPMA mon	metamorphic	Oyhantçabal et al. (2012)
73	UY08-8	31°34′35.67"S	55°34′11.76"W	2094	17	Mesocratic gneiss	Rivera Granulitic Complex	Pb–Pb titanite	metamorphic	Oyhantçabal et al. (2012)
74	UY08-8 (1)	31°34′35.67"S	55°34′11.76"W	2114	3.1	Mesocratic gneiss	Rivera Granulitic Complex	U–Pb SHRIMP zircon	magmatic	Oyhantçabal et al. (2012)
75	UY08-8 (2)	31°34′35.67"S	55°34′11.76"W	2147	8.7	Mesocratic gneiss	Rivera Granulitic Complex	U–Pb SHRIMP zircon	magmatic	Oyhantçabal et al. (2012)
76	UY-10-05 (cores)	32°28'45"S	54°28'1.8"W	776	12	gneiss	Cerro Olivo Complex	U–Pb SHRIMP zircon	magmatic	Oyhantcabal et al. (2009)
77	UY-10-05 (rims)	34°28'45"S	54°28'2"W	641	17	gneiss	Cerro Olivo Complex	U–Pb SHRIMP zircon	metamorphic	Oyhantcabal et al. (2009)
78	UY-1-13	33°13′43.41"S	54°43′3.76"W	550.5	2.7	marbles	Las Tetas Complex	Rb-Sr mica + WR isochrone	cooling age	Oriolo et al. (2016b)
79	UY-1-13	33°13′43.41"S	54°43′3.76"W	621.4	1	marbles	Las Tetas Complex	Ar-Ar phlogopite	metamorphic	Oriolo et al. (2016b)

(*continued on next page*)

Table III (*continued*)

#	sample	Latitude	Longitude	Age (Ma)	2σ	Rock-type	Unit	Method	Interpretation	Reference
80	UY-12-05	34°38'2.5"S	55°17'23"W	573	11	pebbly sandstones	Barriga Negra Group	U–Pb SHRIMP zircon	magmatic	Oyhantcabal et al. (2009)
81	UY-13-14	34°53′19.06"S	55° 2′27.31 "W	420	-	granitic mylonite	Sierra Ballena Shear Zone	Ar-Ar amphibole	cooling age	Oriolo et al. (2016b)
82	UY-26-14	34°17′4.97"S	54°37′56.14"W	589.7	6.2	Mylonitic granite	Florencia Granite	K-Ar muscovite	cooling age	Oriolo et al. (2016b)
83	UY-2-A	34°17′44.12"S	54°3 2′7.5"W	771	6	Mafic gneiss	Cerro Bori Orthogneisses	U–Pb SHRIMP zircon	magmatic	Lenz et al. (2011)
84	UY3-05 (1)	31°41′17.43"S	55°24′3.05"W	2093	36	Leucocratic gneiss	Valentines– Rivera Granulitic Complex	U–Pb SHRIMP zircon	magmatic	Oyhantçabal et al. (2012)
85	UY3-05 (2)	31°41′17.43"S	55°24′3.05"W	2172	8	Leucocratic gneiss	Valentines– Rivera Granulitic Complex	U–Pb SHRIMP zircon	magmatic	Oyhantçabal et al. (2012)
86	UY-3-13	33°13′42.76"S	54°42′ 11.02"W	596.8	1.1	Mylonitic gneiss	Maria Albina Shear Zone	Ar-Ar plateau age (Mus)	cooling age	Oriolo et al. (2016b)
87	UY-40-14	33° 9′28.63"S	54°57′52.29"W	600	14	Mylonitic gneiss	La China Complex	Ar-Ar amphibole	cooling age	Oriolo et al. (2016b)
88	UY-41-14	33° 8′25.17"S	55°10′21.98"W	604.9	6.3	quartz-micaschists	Las Tetas Complex	K-Ar muscovite	cooling age	Oriolo et al. (2016b)
89	UY-45-14	33°12′58.26"S	54°41′40.13"W	619.4	8.5	Mylonitic gneiss	Maria Albina Orthogneiss	K-Ar muscovite	cooling age	Oriolo et al. (2016b)
90	UY-48-14	32°48′31.20"S	54°16′12.88"W	615.2	6.6	Mylonitic gneiss	Cerro Amaro Shear Zone	K-Ar muscovite	cooling age	Oriolo et al. (2016b)
91	UY-57-14	32°58′48.57"S	54°37′20.76"W	630.2	6.1	Mylonitic gneiss	Isla Patrulla Shear Zone	Ar-Ar amphibole	cooling age	Oriolo et al. (2016b)
92	UY-6-14	34°33′19.31"S	54°43′24.77"W	632.7	6.1	Mylonitic gneiss	Cordillera Shear Zone	K-Ar muscovite	cooling age	Oriolo et al. (2016b)
93	UY-7-04	34°43′3.60"S	55° 5′31.02"W	564	4.1	amphibolite	Campanero Unit	Ar–Ar hornblende	cooling age	Oyhantçabal et al. (2009)
94	UY-8-05	34°20′30"S	54°34′32"W	614	3.2	granite	Valdivia Granite Complex	Pb–Pb titanite	magmatic	Oyhantçabal et al. (2007)
95	ZAP-20	33°33′34"S	54°55′24"W	3096	45	Migmatite	La China Complex	U–Pb LA-ICP-MS zircon	magmatic	Gaucher et al. (2011)
96	BUY-80-11	33°27′11.87"S	55°18′44.90"W	1768	11	Rapakivi granite	Paleoproterozoic granitoids	U–Pb LA-ICP-MS zircon	magmatic	Oriolo et al. (2019)
97	UC-10	34°26′17.39"S	55°12′38.59"W	1479	4	Metagabbro	Zanja del Tigre Complex	U–Pb LA-ICP-MS zircon	magmatic	Oriolo et al. (2019)
98	UC-11	34°28′59.27"S	55°12′39.17"W	1482	6	Metagabbro	Zanja del Tigre Complex	U–Pb LA-ICP-MS zircon	magmatic	Oriolo et al. (2019)

3. Experimental Design, Materials and Methods

3.1. Sample preparation

The sample preparation comprises the crushing and sieving of rock samples and fine grinding of the resulting products in the standard grain size of zircon ($50<\Phi<300$ microns) and then the separation concentration zircons. The mineral separation laboratory carried out these procedures at the Geochronological Research Center of the Universidade de São Paulo (CPGeo-IGc / USP). The heavy mineral concentrate was obtained using a Wilfley gravitational table, heavy liquids and magnetic separation by hand magnet and Frantz magnetic separator. The resulting impure zircon concentrates were cleaned from their gangue with ultrasound and strong acids, and the concentrated residual fraction was manually trickled under a binocular microscope (BM) by hand-picking. The separated zircons were placed in mounts on epoxy resin. Standard protocols to place grains in the epoxy resin plate were followed. After observation under BM, the resin plate was super-polished to expose the central part of the grains and metallised to be observed by cathodoluminescence in the SEM.

3.2. Optical binocular microscope

The first step in microscopic analysis of zircons is to study them in a Petri dish with ethanol, under a high-resolution binocular microscope, and select and document the grains by photomicrographs. Properties such as colour, degree of transparency, external morphology and crystalline development are observed. The main external characteristics to pick up are (i) length to width aspect ratios, (ii) colour and degree of transparency, (iii) presence of xenocryst cores and inclusions of other minerals, (iv) degree of fracturing and alteration, and (v) crystallographic typology, like the relationship between prismatic vertical axes and pyramidal crystal faces.

3.3. Cathodoluminescence and textural study

Once the zircon mount was made in epoxy resin, the grains are numbered first with the transmission microscope (40x). The mount is placed on the excimer laser microprobe, in which a 15 kV electron beam bombardment generates cathodoluminescence (CL) images. CL imaging is essential to describe textural patterns. Zircon morphology and texture reflect the geological history, especially in magmatic nucleation, overgrowing and metamorphic recrystallisation, deformation, or volume change, and chemical alteration [2].

3.4. LA-ICP-MS U-Pb analytical technique

We set up the isotopic data and zircon dating at the Geochronological Laboratory of the Geosciences Institute from the University of São Paulo (Brazil). The LA-ICP-MS equipment locates at the CPGeo-IGc/USP and has an excimer laser of ArF gas (193 nm) coupled to the Neptune^{TM} High-Resolution Multi-collector ICP-MS. The excimer laser used here provides a better regularity of abrasion, reducing the fractionation between masses due to its high optical quality and source stability [3]. The ICP-MS analytical procedure calibrates using the international standard zircon Temora-1 standard zircon ($^{206}Pb/^{238}U = 0.06683$). Results are displayed in $^{206}Pb/^{238}U$ vs $^{207}Pb/^{235}U$ Wetherill's Concordia diagram and $^{206}Pb/^{238}U$ vs $^{207}Pb/^{206}Pb$ Tera-Wasserburg's graph, using IsoplotR [4]. Wetherill's Concordia diagrams served both to model magmatic protoliths' concordant age and the systematic radiogenic lead loss due to subsequent geological processes. The zircons were ablated during 40 seconds in the 193 nm Excimer Laser Ablation

System, at 7-6 Hz, 6mJ and full energy, obtaining spots of ca. 25 μm (Helium: MFC1 = 0.300 L/min, MFC2 = 0.300 L/min, Argon: Aux.= 0.95 L/min, sample = 0.978 L/min).

4. Figures and Tables

4.1. Petrographic data

The petrographic data corresponding to section 1 is commented on the following captions and documented on the photographic and photo-micrographic plates (Figs. 2–8).

4.2. U-Pb Isotopic data of zircons

Table I contains the isotopic results obtained in the U-Pb Geochronology Laboratory of the University of Sao Paulo between 2016 and 2017 from two sample sets. It contains the isotopic ratios of U and Pb commonly used to calculate the absolute ages $T^{238}U/^{206}Pb$, $T^{235}U/^{207}Pb$ and $T^{207/206}Pb$. There are the results of concordant and isochronal ages of radiogenic Pb loss for the six dated samples in the last column. Although the results of the isotopic ratios present uncertainties obtained at one sigma, the calculations of the ages with the Vermeesch's Isoplot-R software [4] were calculated at two sigmas.

Table II contains a comparative analysis of the different internal textures of the dated zircons from each of the six samples in this study. The items considered for the correlation were the external morphological aspects, the internal texture subdivision in (i) core, (ii) rim, and (iii) other diagnostic features due to the crystallisation/recrystallisation of the grains. We consider it a priority to evaluate the presence of overgrowth, transgressive replacement fronts, inclusions, fracturing, and alteration linked to the damage caused by radiation. The Th/U ratio was also evaluated. All the samples except one presented inheritance of Archean ages.

Table III compilation of antecedents related to absolute ages by the U-Pb method in zircon from the central-eastern and south-eastern region of Uruguay. It is an exhaustive list of antecedents to date, understanding that the rapid evolution of geochronological knowledge in this region requires a continuous review of published data. Although the list refers exclusively to the U-Pb data, a single Rb-Sr isochronal age antecedent (corresponding to the Umpierre & Halpern's document of 1971) was included and considered a valuable antecedent for the dating of the "Illescas Granite". The advantage of this table is that it presents the Latitude - Longitude coordinates collected and recalculated from the consulted works.

4.3. Supplementary data

Table III

Ethics Statement

- This material is the authors' original work, which has not been previously published elsewhere.
- The authors did not submit this paper for other publication elsewhere.
- The paper reflects the authors' research and analysis wholly and truthfully.
- The paper properly credits the meaningful contributions of co-authors and co-researchers.
- The results are appropriately placed in the context of prior and existing research.
- All sources used are correctly disclosed (correct citation).

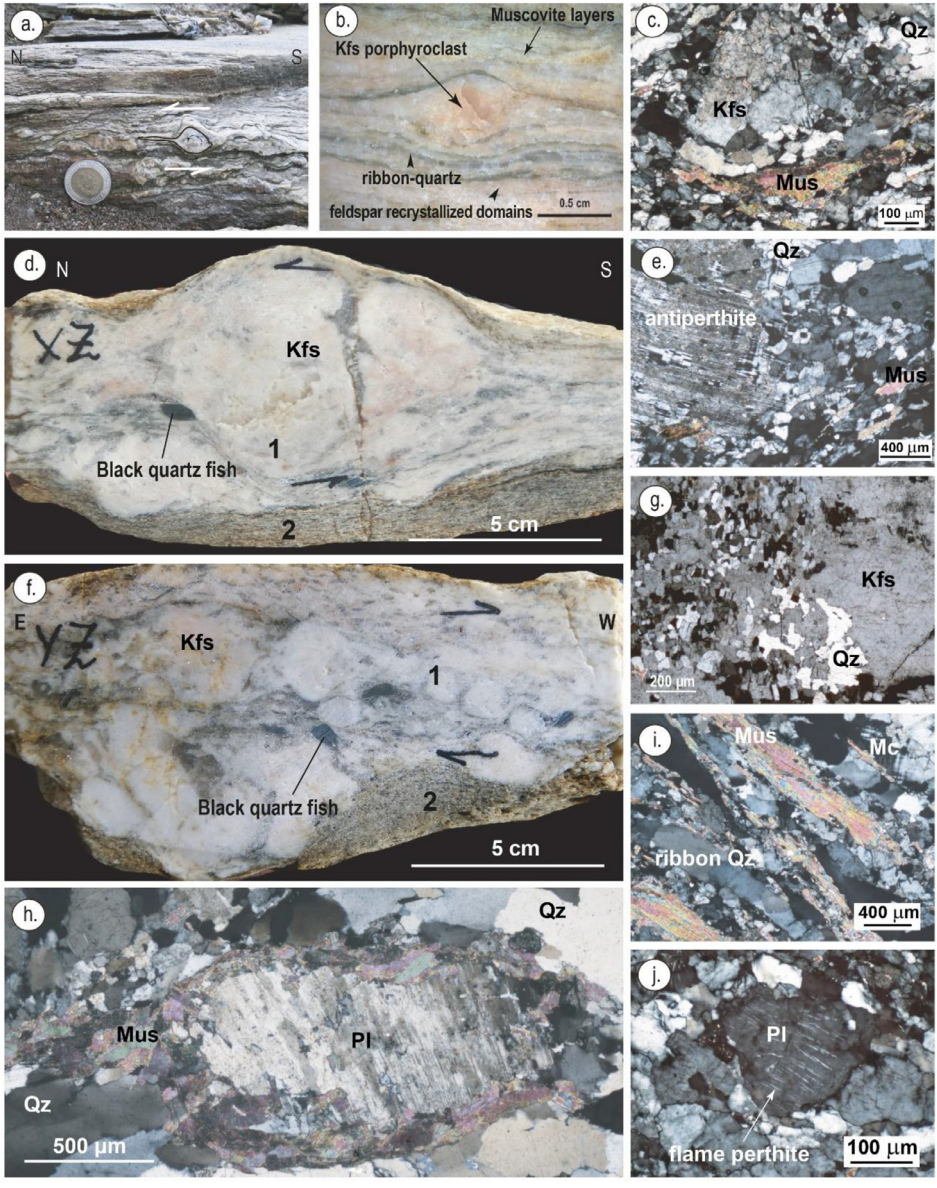

Fig. 8. Flat-lying muscovite augen gneiss (Mi06) in the "Zapican Thrust", a) Mylonitic foliation (coin is 2.5 cm). b) K-feldspar porphyroclast. c) Phenocryst *vs* matrix. d) Section in XZ plane and sinistral shear. e) Phenocryst of patchy antiperthitic plagioclase. f) Section in YZ plane and dextral shear. g) Partial recrystallisation of Kfs phenocryst. h) Antiperthitic porphyroclast surrounded by muscovite. i) Detail of muscovite layers and ribbon quartz. j) Flame perthite in plagioclase.

- All authors have been personally and actively involved in substantial work leading to the paper and will take public responsibility for its content.
- No information obtained for experimentation with human subjects was used.
- No information obtained for experimentation with animals was used.

CRediT Author Statement

Henri Masquelin: Conceptualisation, Methodology, Software, writing-original draft preparation; **Tahar Aïfa:** Data curation, Software, Writing - original draft preparation; **Fernando Scaglia:** Visualization, Investigation; **Miguel Basei:** Data curation, software, Validation.

Declaration of Competing Interest

The authors declare that they have no known competing financial interests or personal relationships which have or could be perceived to have influenced the work reported in this article.

Acknowledgments

We are indebted to the Director Lic. Nestor Campal authorised the use of the airborne geophysical data of DINAMIGE for academic purposes. We also thank Bruna Sanches, Nairé Gabriel, and the rest of the team at the Centro de Pesquisas Geocronologicas of the University of São Paulo. We thank Dr Elena Peel for the help regarding the use of standard deviation in the Concordia diagram. The authors are grateful to CSIC (UdelaR) for the funding granted (first author's project CSIC-2015 C-604) and to the Faculty of Sciences of the Universidad de la República (Uruguay) for the Logistics. They also acknowledge PEDECIBA - Geosciences, who provided third author's grants. To Ecos-sud Conicyt program n°U17U01 for funding the travels and per diem to Tahar Aïfa and Henri Masquelin through a cooperation exchange program between the Rennes 1 and UdelaR universities since 2018. This work is also a contribution to the Unesco-igcp638 program.

References

[1] C.W. Passchier, R.A. Trouw, Microtectonics, Springer Science & Business Media, 2005.
[2] M.J. Kohn, N.M. Kelly, Petrology, and geochronology of metamorphic zircon, In Moser et al. (eds.), chapter 2, Microstructural geochronology: Planetary records down to atom scale, Geophysical Monograph Series, AGU, 2018, 35-61.
[3] K. Sato, M.A.S. Basei, O. Siga Júnior, W.M. Sproesser, A.T. Onoe, Excimer laser (193 nm) acoplado ao ICP-MS Neptune: primeiros resultados de análises isotópicas, in: Simpósio 45 Anos de Geocronologia no Brasil, Resumos Expandidos, 2009, pp. 131–133. USP.
[4] P. Vermeesch, IsoplotR: a free and open toolbox for geochronology, Geosci. Front. 9 (5) (2018) 1479–1493.
[5] D.L. Whitney, B.W. Evans, Abbreviations for names of rock-forming minerals, Am. Mineralogist 95 (1) (2010) 185–187.
[6] L. Sánchez Bettucci, F. Preciozzi, M.A.S. Basei, P. Oyhantçabal, E. Peel, J. Loureiro, Campanero Unit: a probable Paleoproterozoic basement and its correlation to other units of south-eastern Uruguay, in: IV South American Symposium on Isotope Geology, Short Papers, CBPM; IRD, Salvador, 2003, pp. 673–674.
[7] H. Masquelin, L.A. D'Avila Fernandes, C. Lenz, C.C. Porcher, N.J. McNaughton, The Cerro Olivo complex: a pre-collisional Neoproterozoic magmatic arc in Eastern Uruguay, Int. Geol. Rev. 54 (10) (2012) 1161–1183.
[8] C. Lenz, L.A.D. Fernandes, N.J. McNaughton, C.C. Porcher, H. Masquelin, U–Pb SHRIMP ages for the Cerro Bori Orthogneisses, Dom Feliciano Belt in Uruguay: evidence of a ca. 800 Ma magmatic and ca. 650 Ma metamorphic event, Precambrian Res. 185 (3–4) (2011) 149–163.
[9] H. Masquelin, in: Evolução estrutural e metamórfica do Complexo Gnáissico Cerro Olivo, Sudeste do Uruguay, Tese de Doutorado, CPGeo - UFRGS, 2002, pp. 1–344. 1 map.
[10] E. Peel, L.S. Bettucci, M.A.S. Basei, Geology and geochronology of Paso del Dragón Complex (north-eastern Uruguay): implications on the evolution of the Dom Feliciano Belt (Western Gondwana), J. South Am. Earth Sci. 85 (2018) 250–262.
[11] C. Gómez Rifas, in: A zona de cisalhamento sinistral de Sierra Ballena no Uruguai, Tese de doutorado, IG–USP, São Paulo, 1995, pp. 1–243. 5 maps.
[12] P. Oyhantçabal, S. Siegesmund, K. Wemmer, S. Presnyakov, P. Layer, Geochronological constraints on the evolution of the southern Dom Feliciano Belt (Uruguay), J. Geol. Soc. 166 (6) (2009) 1075–1084.